# Quantum Hall effect and general narrow-wire circuits

R. L. Schult, H. W. Wyld, and D. G. Ravenhall
*Department of Physics, University of Illinois at Urbana-Champaign, 1110 West Green Street, Urbana, Illinois 61801*
(Received 13 November 1989)

A theoretical study is made of charged-particle motion in planar circuits made up of narrow wires, in the presence of a magnetic field of arbitrary strength, in the ballistic approximation. The basic element is a four-terminal junction of narrow wires, and its detailed properties are calculated. Its scattering probabilities strongly reflect the influence of quantum effects of the junction, including subband thresholds and virtual, resonant states, and the Hall resistance calculated from them may depart considerably from the classic wide-wire result. Physical features are related to the emergence of pinned Landau levels as the field strength increases. By suitably modifying the four-terminal method, it is extended to include elbow (L) and tee (T) junctions. The results are then used to construct linear six- and eight-terminal junctions, whose resistive properties are discussed. The Hall resistance is predicted to depend on which arms are used and on the stub spacing. The application of the method to the general linear series of junctions is then outlined. The four-terminal results are also applied to a square eight-terminal junction, to show the presence and the consequences of the Aharonov-Bohm effect in circuits with closed loops.

## I. INTRODUCTION

There is considerable current experimental[1–7] and theoretical[8–13] interest in the physics of quantum wires, devices made to conduct along two-dimensional surfaces shaped into very narrow channels. The quantum Hall effect observed when such devices are placed in a magnetic field perpendicular to the plane is modified, compared with the classic wide-sample case,[14] by the quantum interference effects such narrow channels exhibit. Theoretically, the simplest such device is the four-terminal junction (Fig. 1), but in practice it is usual to construct more complicated circuits, by combining elements that have that basic geometry. The finite width $w$ of the wires results in a transverse quantization, so that electrons populate subbands whose threshold energies depend on $w$ and on $B$, the strength of the magnetic field. For large $w$, and a Fermi energy and $B$, such that $n_0$ subbands are open, one expects a Hall resistance $R_H = h/(e^2 n_0)$.[1,14] For small $w$, however, the experimental results deviate from this prediction,[1–7] and attempts to understand these deviations have been made by Peeters[9] and by Büttiker[15] and others.[10–13] We have presented in an earlier paper[10] our results on the properties of the four-terminal junction that make no assumptions except the ballistic approximation, and we here document the methods that produced them, and then apply these methods to more general circuits. The method can be used for any circuit that can be made from rectangles. It is not directly applicable to the case of adiabatically widened channels, which seems quite important[13] for understanding generic "quenching"[1] of $R_H$ at low fields.

We present in Sec. II a complete quantum-mechanical treatment of the four-terminal junction. As is discussed in Secs. III and IV, such a treatment[16] predicts, for zero $B$ field, bound states at the junction, and also rapid variations with energy of the scattering probabilities (the quantities that in the ballistic approximation determine $R_H$) at the thresholds for the opening of new channels (subbands). This complexity is enhanced by the presence of a magnetic field. New structures arise at certain energies, causing $R_H$ to go through zero there. These structures are associated with virtual or resonant junction states which become, in the limit of large $B$, two-dimensional Landau levels pinned to the junction.[10] The suggestion that resonances at the junction might be important was made in Ref. 1, and a comment by Roukes (private communication), suggesting that there might be

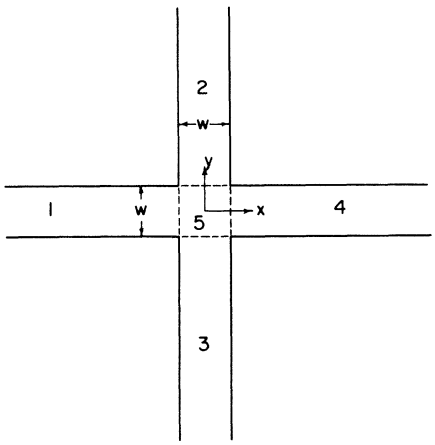


FIG. 1. Schematic representation of the four-terminal junction of wires of width $w$. The particle potential is zero inside the wires, and infinite outside. The five regions in which wave functions are represented by sums in Sec. II C are indicated. The sums are to be matched across the boundaries represented by the dashed lines.

 

a bound state as well, was the original impetus for our work in this area.

We also discuss the extension of these methods to compound circuits. Straightforward truncation of the matrix introduced in Sec. II allows us to include elbows ("L") and tees ("T") in circuits, and sample properties of these elements are given. We discuss the phases and gauge transformations involved in considering all possible positions and orientations of such junctions. Section III develops a method to concatenate them into six-, eight-, and $n$-terminal collinear junctions. It also considers the square loop circuit. The results for the loop, with its very sharp "resonances," are discussed also in terms of the wave functions of the whole loop and their symmetries.

## II. THE FOUR-TERMINAL JUNCTION

The basic element of our circuit calculations is the four-terminal junction, and we wish to present in detail the calculation of its properties. Our method[10,16] consists in matching, on the periphery of the square defining the intersection (the dashed lines in Fig. 1), functions that solve the single-wire problem. Although some of those functions have been introduced earlier, by Peeters,[9] we discuss them again for completeness, and because we need a complete set of channel states, including the evanescent ones.

### A. Schrödinger's equation

States for vertical arms such as arm 2 of Fig. 1 are obtained most conveniently by using the vector potential $\mathbf{A}=(0,Bx,0)$ to represent the effect of a uniform field $B$ in the positive $z$ direction. The Schrödinger equation for a particle of mass $m$, charge $q$, and energy $E=\hbar^2k^2/2m$ is then

$$\left[-\left[\frac{1}{i}\nabla-\frac{q}{\hbar c}\mathbf{A}\right]^2+k^2\right]\psi(x,y)=0\ . \tag{2.1}$$

It may be solved in the separable form[17]

$$\psi_p(x,y)=e^{ipy}f_p(x)\ , \tag{2.2}$$

where $f_p(x)$ satisfies

$$\left[\frac{d^2}{dx^2}+k^2-\left[\frac{x}{l^2}-p\right]^2\right]f_p(x)=0\ . \tag{2.3}$$

Here $l$ is the magnetic length defined by $1/l^2=qB/\hbar c$. (That quantity is positive if $qB>0$.) For an infinite $(x,y)$ space, $f_p(x)$ is a harmonic-oscillator state shifted from $x=0$ by an amount $pl^2$, and there is a continuum of (real) $p$ values and states $\psi_p(x,y)$. We assume infinite wall boundary conditions, i.e., for the channel of width $w$, the differential equation must be solved with the boundary conditions $f_p(w/2)=f_p(-w/2)=0$. This boundary-value problem defines for each value of $k^2$ a discrete set of eigenvalues $p_m$ and corresponding functions $f_{p_m}(x)$, which we will sometimes call $f_p(x)$ or $f_m(x)$, where $m$ enumerates the discrete set. For the limit $B=0$ these functions become[16]

$$f_m(x)=\sin[(m\pi/w)(x+w/2)]\ , \tag{2.4}$$

with $p_m^2=k^2-(m\pi/w)^2$. For nonzero $B$ they are each an awkward combination of Kummer functions that depends on the two dimensionless parameters $kw$ and $l^2/w^2$. We have found it convenient to obtain the eigenvalues $p_m$ and the functions $f_{p_m}(x)\equiv f_p(x)\equiv f_m(x)$ directly, by numerical solution of the differential equation.

There are two symmetries that relate pairs of the functions $f_p(x)$. First, the differential equation for $f_p(x)$ is invariant if $p$ and $x$ are replaced by $-p$ and $-x$, respectively. Thus, the equation for $f_{-p}(x)$ is the same as that for $f_p(-x)$ and these functions can differ only in phase. We choose the phase to be

$$f_{-p_m}(x)=(-1)^{m-1}f_{p_m}(-x) \tag{2.5}$$

as the natural extension of the choice for the $B=0$ case. The second symmetry relates $p$ and its complex conjugate $p^*$. Taking the complex conjugate of Eq. (2.3) we see that the relationship is

$$f_{p^*}(x)=\eta_p[f_p(x)]^*\ , \tag{2.6}$$

where $\eta_p$ is a complex phase factor. The natural choice $\eta=1$ makes $f_p(x)$ real for real $p$. When $p$ is purely imaginary the two symmetries together make (for $\eta_p=1$)

$$\begin{aligned}&\mathrm{Re}f_p(x)=(-1)^{m-1}\mathrm{Re}f_p(-x)\ ,\\ &\mathrm{Im}f_p(x)=(-1)^m\mathrm{Im}f_p(-x)\quad(\text{if } p^*=-p)\ .\end{aligned} \tag{2.7}$$

When $p$ is neither purely real nor purely imaginary, the four values $p$, $-p$, $p^*$, and $-p^*$ are all distinct but the four corresponding $f_p$'s are all related by these two symmetries.

### B. Orthogonality and normalization

Standard application of the Sturm-Liouville analysis shows that two functions $f_{p_n}(x)$ and $f_{p_m}(x)$ belonging to the same $k^2$ satisfy

$$(p_n-p_m)I_{p_np_m}\equiv(p_n-p_m)\int_{-w/2}^{w/2}dx\, f_{p_m}(x)f_{p_n}(x)(p_n+p_m-2x/l^2)=0\ . \tag{2.8}$$

Thus whenever $p_n \neq p_m$, the functions are orthogonal in the sense that

$$I_{p_n p_m} = 0, \quad p_n \neq p_m \ . \tag{2.9}$$

For reasons discussed in the following paragraph we choose to normalize our functions $f_p(x)$ so that

$$I_{pp} = \frac{p}{|p|} \ . \tag{2.10}$$

Note that this specifies not only the magnitude but also the phase (up to a possible minus sign ) of $f_p(x)$ since $I_{pp}$ involves the square rather than the absolute value of $f_p(x)$.

Since the peculiar weighting in the orthogonality integral $I_{p_n p_m}$ involves the eigenvalues $p_n$ and $p_m$, it is not particularly useful as a projection operator. It is useful, however, in evaluating the flux of electrons along the channel, as obtained by integrating, across the channel, the usual expression for current density along the channel, i.e.,

$$J_y = \frac{1}{2m} \int dx \left[ \psi^*(x,y) \left( -i\hbar \frac{\partial}{\partial y} - \frac{q}{c} A_y \right) \psi(x,y) + \psi(x,y) \left( i\hbar \frac{\partial}{\partial y} - \frac{q}{c} A_y \right) \psi^*(x,y) \right] . \tag{2.11}$$

When $\psi(x,y)$ is represented as a sum

$$\psi(x,y) = \sum_m \gamma_m f_m(x) e^{ip_m y} \ , \tag{2.12}$$

the integrals can be reduced, using the symmetry (2.6), to $I_{p_n p_m}$ with the result that for our normalization of $f_p(x)$, the flux is proportional to $\sum_p (\gamma_{(p^*)})^* \gamma_p p/|p|$ with no extra velocity factor. Single complex $p$'s do not contribute to net flux, although two evanescent waves with wave numbers $p$ and $p^*$ can interfere to give the same type of flux as in the usual barrier penetration case.

For each nodal number $m$ there is a band of values of $k^2$ for which $p_m$ is real and the states $\psi_m$ are propagating states. At the band edge, $k^2 = k_m^2$, the lowest $k^2$ for which $p_m$ is real, the eigenvalue $p_m$ is zero. The band edges depend on $B$: for $B = 0$, $k_m = m\pi/w$, while for large $B$, $k_m \to (2m-1)^{1/2}/|l|$. The dependence of $k_m^2$ on the dimensionless quantity $\mathcal{B} = w^2/l^2$ is shown in Fig. 2. For a Fermi energy $E_F = \hbar^2 k_F^2/2m$ such that $k_{n_0} < k_F < k_{n_0+1} < k_F < k_{n_0+1}$ there are $n_0$ one-dimensional Fermi gases, each of which contains momentum states that extend from $-p_m$ to $p_m$, where $p_m$ is the eigenvalue associated with $k_F$ and the nodal state $m$.

For any given value of $k^2$ and $B$, the set of $p_m$'s includes in addition to these real values (propagating nodes), purely imaginary values (evanescent or damped modes) and/or complex values (oscillatory damped modes). At $B = 0$, $p_m^2 = k^2 - m^2\pi^2/w^2$ and $p_m$ is either purely real or purely imaginary. For nonzero $B$, complex values of $p_m^2$ may also arise. For example, at $kw = 9.5$,

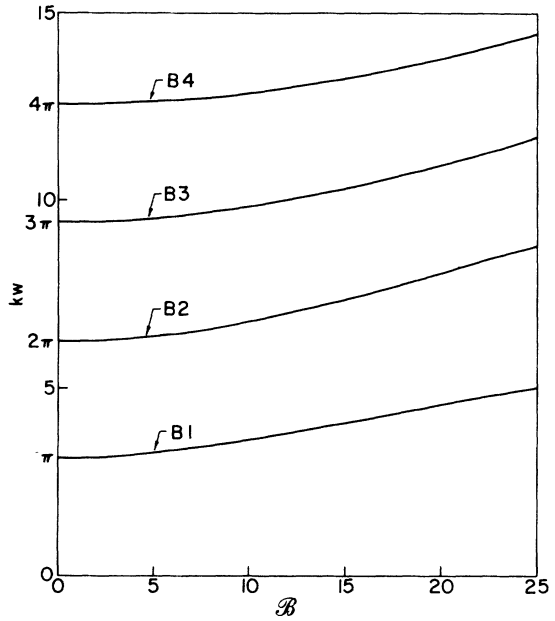


FIG. 2. The values of $kw$ for the first four band edges, as a function of the dimensionless quantity $\mathcal{B} = w^2/l^2 = w^2 eB/\hbar c$.

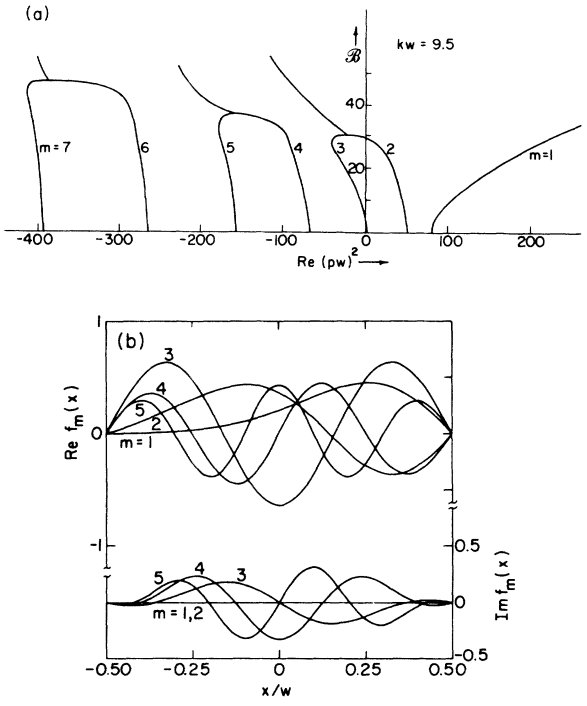


FIG. 3. Information about the single-wire wave functions: (a) $\mathrm{Re}(pw)^2$, where $pw$ is the dimensionless quantity proportional to the longitudinal momentum, as a function of the dimensionless quantity $\mathcal{B}$, for $kw = 9.5$. At $\mathcal{B} = 0$, the values of $(pw)^2$ are $(kw)^2 - (m\pi)^2$, for the solutions $\psi_m$. The imaginary parts of $(pw)^2$ are zero until the curves for neighboring $m$ values coalesce. (b) The real and imaginary parts of the functions $f_m(x)$, for $kw = 9.5$ and $\mathcal{B} = 10$. For $m = 1$ and 2, the imaginary parts are zero.

the real part of $(p_m w)^2$ is given as a function of $\mathcal{B}$ in Fig. 3(a). We note that the values of $p_m^2$ decrease as $m$ increases. The values of $p_m$ for $m > n_0$ are therefore complex. States with imaginary parts to $pw$ comprise the evanescent states needed to represent the exact wave function near the junction. We find numerically that $(pw)^2$ is real if $\mathcal{B}$ ($\equiv w^2/l^2$) is $\lesssim 30$ (for $kw = 9.5$). Under this condition $pw$ is either pure real or pure imaginary. For larger $\mathcal{B}$ the behavior is more complicated. The maxima of pairs of values of $(pw)^2$ in the figure actually represent thresholds for complex $(pw)^2$, at which $\mathcal{B}$ the purely imaginary $pw$ acquire also a real part. For all of these evanescent states the corresponding functions $f_m(x)$ are also complex. For the particular values $\mathcal{B} = 10$ and $kw = 9.5$, we plot in Fig. 3(b) the first few eigenfunctions $f_m(x)$.

### C. Gauge dependence and rotations

The functions described earlier were obtained in the special gauge useful for vertical arms. We can convert to any other gauge by multiplying by the phase factor $e^{iq\phi(x,y)/\hbar c}$ where the new vector potential $\mathbf{A}_{\text{new}} = A_{\text{old}} + \nabla\phi$. Thus to transform to the symmetric gauge $\mathbf{A} = (-By/2, Bx/2, 0) = (0, Bx, 0) + \nabla(-xyB/2)$ we need only multiply by

$$e^{-ixy/(2l^2)} . \tag{2.13}$$

To obtain the states for the horizontal arms such as arm 4 in Fig. 1, the vector potential $\mathbf{A} = (-By, 0, 0)$ allows a similar separation of variables. In terms of the functions $f_p$ already defined, such a wave function is

$$\Psi_p(x,y) = e^{ipx} f_{-p}(y) , \tag{2.14}$$

i.e., the function which confines the wave to the channel with $-w/2 < y < w/2$ when the wave is traveling with wave number $p$ in the $x$ direction involves $-p$, not $p$. Physically, a particle with positive charge $q$ traveling upwards with wave number $p$ in $y$ is pushed to the right-hand side of the channel, i.e., towards $x = w/2$, as is seen for the $m = 1$ state in Fig. 3(b). Evidently, when this particle moves in the $x$ direction with wave number $p$ it is pushed to its right also, which now corresponds to $y = -w/2$. A particle moving with $-p$ in the $x$ direction will be pushed towards $y = +w/2$.

We have then, in the various regions of Fig. 1, the following wave functions. The wave function in region 2, chosen to have only outgoing waves, is

$$\Psi_2(x,y) = e^{-ixy/(2l^2)} \sum_{m=1}^{M} \gamma_m e^{ip_m y} f_m(x) , \tag{2.15}$$

where the constant coefficients $\gamma_m$ are yet to be determined. For $n_0 < m < M$, where $p_m^2 < 0$ or is complex, the imaginary part of $p_m$ is $> 0$. The sum up to $m = M$ contains, therefore, only outgoing waves and as many exponentially decaying waves as are needed to make an accurate fit at the junction. In region 4 the wave function with only outgoing waves is

$$\Psi_4(x,y) = e^{ixy/(2l^2)} \sum_{m=1}^{M} \beta_m e^{ip_m x} f_{-m}(y) . \tag{2.16}$$

In region 3 the wave function is of similar kind to $\Psi_2$, involving coefficients $\delta_m$. In region 1, the arm that contains incoming waves in the open channels, the wave function must be

$$\Psi_1(x,y) = e^{ixy/(2l^2)} \sum_m [\alpha_m e^{-ip_m x} f_m(y) + \alpha'_m e^{ip_m x} f_{-m}(y)] , \tag{2.17}$$

where, as described earlier, $f_{-m}(y)$ means the solution with momentum $-p_m$, and for an isolated four-terminal junction $\alpha'_m = 0$ for $m > n_0$ (i.e., there are incident waves only in the propagating modes). In region 5, the intersection requires waves of all types:

$$\Psi_5(x,y) = e^{ixy/(2l^2)} \sum_m [\epsilon_m e^{-ip_m x} f_m(y) + \epsilon'_m e^{ip_m x} f_{-m}(y)] + e^{-ixy/(2l^2)} \sum_m [\xi_m e^{ip_m y} f_m(x) + \xi'_m e^{-ip_m y} f_{-m}(x)] . \tag{2.18}$$

Note that the first two terms represent a function which is zero at $y = \pm w/2$ but can describe an arbitrary function at $x = \pm w/2$ while the last two terms are zero at $x = \pm w/2$ and represent an arbitrary function along $y = \pm w/2$. Taken together they describe a solution of the Schrödinger equation in region 5 that can be arbitrarily specified along the boundaries of region 5. All of these wave functions $\Psi$ are solutions of the Schrödinger equation (2.1), with the symmetric gauge $\mathbf{A} = (-By/2, Bx/2, 0)$.

### D. Matching

The wave functions and their normal derivatives are to be matched at the edges of the square, shown in Fig. 1; a procedure which equates eight sets of sums over modes. Since, as mentioned earlier, the functions $f_m(x)$ do not possess a simple orthogonality property, the procedure of multiplying by a specific function $f_m(x)$ (or its complex conjugate) and integrating over the side of the square to reduce these sum equations to a matrix equation whose elements involve individual modes may be done in a variety of ways. All of those we have tried are found to produce the same amplitudes. A judicious choice of the multiplying function for each equation reduces the integrals involved to

$$
\begin{aligned}
A_{m'm} &= \int_{-0.5}^{0.5} (dy/w) f_{-m'}(y) e^{iyw/4l^2} f_{-m}(y) \,, \\
B_{m'm} &= \int_{-0.5}^{0.5} (dy/w) f_{-m'}(y) e^{iyw/4l^2} f_{m}(y) \,, \\
C_{m'm} &= \int_{-0.5}^{0.5} (dy/w) f_{-m'}(y) e^{iyw/4l^2} (ip_m + iy/2l^2) f_{-m}(y) \,, \\
D_{m'm} &= \int_{-0.5}^{0.5} (dy/w) f_{-m'}(y) e^{iyw/4l^2} (-ip_m + iy/2l^2) f_{m}(y) \,, \\
E_{m'm} &= \int_{-0.5}^{0.5} (dy/w) f_{-m'}(y) e^{-iyw/4l^2} e^{ip_m y} \,, \\
F_{m'm} &= \int_{-0.5}^{0.5} (dy/w) f_{-m'}(y) e^{-iyw/4l^2} e^{-ip_m y} \,.
\end{aligned}
\tag{2.19}
$$

where $m, m' = 1 \cdots M$. In the presence of a nonzero $B$ field these are all independent integrals. In terms of these integrals [or others which reduce to them by use of the symmetry properties of $f_m(y)$], the matching procedure then produces $8M$ equations, $2M$ for each edge, which relate the outgoing waves, with coefficients $\alpha_m \cdots \delta_m$, and the interior waves, $\epsilon_m \cdots \zeta'_m$, to the incoming waves $\alpha'_m$. The $8\times 8$ matrix equation (suppressing reference to modes) is then

$$
\begin{bmatrix}
-q\phi A & 0 & 0 & 0 & q\phi A & q\chi B & 0 & 0 \\
0 & -\phi A & 0 & 0 & \chi B & \phi A & 0 & 0 \\
0 & 0 & -q\phi A & 0 & 0 & 0 & q\phi A & q\chi B \\
0 & 0 & 0 & -\phi A & 0 & 0 & \chi B & \phi A \\
-q\phi C & 0 & 0 & 0 & q\phi C & q\chi D & qf'_-(+)F & qf'_+(+)E \\
0 & -\phi C & 0 & 0 & \chi D & \phi C & f'_+(+)E & f'_-(+)F \\
0 & 0 & q\phi C & 0 & qf'_-(-)E & qf'_+(-)F & -q\phi C & -q\chi D \\
0 & 0 & 0 & \phi C & f'_+(-)F & f'_-(-)E & -\chi D & -\phi C
\end{bmatrix}
\begin{bmatrix} \alpha \\ \beta \\ \gamma \\ \delta \\ \epsilon \\ \epsilon' \\ \zeta \\ \zeta' \end{bmatrix}
=
\begin{bmatrix} q\chi B\alpha' \\ 0 \\ 0 \\ 0 \\ q\chi D\alpha' \\ 0 \\ 0 \\ 0 \end{bmatrix} ,
\tag{2.20}
$$

where $\phi = \exp(ip_m w/2)$, $\chi = \phi^{-1}$, $q = (-1)^{m'-m}$, and the other factors are slopes: $f'_{\pm}(\pm) = f'_{\pm m}(\pm w/2)$. The first four rows come from matching the wave functions on the sides 1, 4, 2, and 3 of the square, respectively, and the second four are for matching derivatives on those same sides. The scattering or $S$ matrix, which expresses the outgoing waves with coefficient $\alpha_m, \beta_m, \gamma_m, \delta_m$ in terms of the incoming waves $\alpha'_m$, then follows from inverting this $8M \times 8M$ matrix.

From the resulting amplitudes, one immediately obtains the probabilities for scattering from incident open channel $m'$ to final open channel $m$ forwards ($F_{mm'}$), sideways to the right ($S_{Rmm'}$), sideways to the left ($S_{Lmm'}$), and backwards by reflection ($R_{mm'}$).

The practicability of this method rests on its convergence properties. We gauge these mainly by how well unitarity at the junction is obeyed. The relationship should be $\sum_n (R_{nn'} + F_{nn'} + S_{Rnn'} + S_{Lnn'}) = 1$. For $M = 6$, unitarity may be violated in the third decimal place for $kw$ values close to the band edge. For the results presented in this paper, we characteristically use $M = 16$, and occasionally see unitarity violated by one or two parts in the fourth decimal place. This is clearly of no practical consequence. The rather slow convergence with $M$ that these results imply is, we believe, caused by the sharp corners assumed for the confining potential, Fig. 1. As we discussed in the case of zero field,[16] a mapping argument shows that the wave function near a corner must behave like $(r - r_c)^{2/3}$. Thus its slope at the corner is infinite. It is the attempt to represent this behavior in terms of channel functions, which have finite slope at the edges, that causes the slow convergence.

## III. MULTITERMINAL JUNCTIONS

### A. Elbows and tees

Because of its symmetry, the four-terminal junction requires the calculation of scattering amplitudes for waves incident in only one arm. The symmetry then tells us the amplitude for waves in other arms. By removing one or two arms of that object, we obtain tee ("T") or elbow ("L") junctions. For these, however, the unsymmetry of the resulting junction, and the presence of a $B$ field, means that several incident-wave situations are needed. We enumerate the possibilities in Fig. 4.

It suffices to describe the procedure for the tee junction

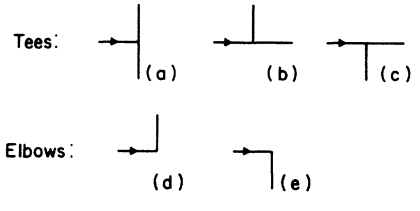


FIG. 4. Amputated versions of the four-terminal junction, representing different incident-wave situations with the tee ("T") and the elbow ("L"). For nonzero $\mathcal{B}$ these all have different wave functions.

TABLE I. Phases of amplitudes for a rotated four-terminal junction. The results of Sec. III refer to an incident wave in arm 1 (see Fig. 1). The phase factor, mode dependent, is $q=(-1)^{m-1}$ and should multiply the amplitudes of Sec. III on the incident and/or the outgoing side according to the entry in the table.

| Incident wave | Rotation | Phase Factors Inc. | Ref. | Trans. | $S_{\text{right}}$ | $S_{\text{left}}$ |
|---|---|---|---|---|---|---|
| 1 | 0 | 1 | 1 | 1 | 1 | 1 |
| 3 | $\pi/2$ | $q$ | $q$ | $q$ | 1 | 1 |
| 4 | $\pi$ | $q$ | $q$ | $q$ | $q$ | $q$ |
| 2 | $3\pi/2$ | 1 | 1 | 1 | $q$ | $q$ |

of Fig. 4(a). The calculation of its wave functions differs from that for the four-terminal junction in that it lacks arm 4, and consequently the derivative across the 5:4 side of the square is not constrained. In terms of the matrix equation (2.20), we must therefore omit the constants $\beta_m$ and the second column; and we must omit the sixth $(=4+2)$ equation, i.e., the sixth row. The $7M\times 7M$ set of equations then yields the outgoing waves $\alpha_m$, $\gamma_m$, and $\delta_m$ in terms of the incident wave $\alpha'_m$.

### B. Phase factors for the general circuit

The solution of the quantum-mechanical problem of motion in a more complicated circuit, such as the six-terminal junction shown in Fig. 5(a), is clearly soluble by application of the same methods as we have used for the four-terminal junction. However, it is not necessary to repeat the whole procedure. It will turn out that for circuits that involve only repetitions of the four-terminal junction or its truncations, the wave functions and scattering amplitudes in all arms may be obtained from those already obtained for those junctions, by iterative procedures following the insertion of crucial phase factors. One complication, which rotational symmetry allowed us to bypass in the case of the four-terminal junction, is the need for wave functions corresponding to incident waves in each of the external channels. For the six-terminal junction, that same symmetry will allow us to equate probabilities of scattering for incident waves in arms 4, 5, and 6 to those with incident waves in arms 3, 2, and 1, respectively. But we do need the wave functions for the three separate incident waves in arms 3, 2, and 1.

First, we observe that the four-terminal wave functions we obtained, which relate outgoing waves in all the arms to incoming waves in only one arm, are special in that the incoming wave was in arm 1, i.e., $x\to-\infty$. One could redo that problem with incoming waves in each of the other arms. But the equivalent result can be obtained by applying a rotation to the system of wave functions we already have. Rotation of $\pi/2$ about the origin is equivalent to the transformation $\hat{\mathbf{i}}\to\hat{\mathbf{j}},\hat{\mathbf{j}},\to-\hat{\mathbf{i}}$ (where $\hat{\mathbf{i}}$ and $\hat{\mathbf{j}}$ are the unit vectors along the $x$ and $y$ axes) and $x\to y, y\to -x$. This clearly leaves the symmetric gauge $\mathbf{A}=(-By/2, Bx/2, 0)$ unchanged. It is physically clear that the *probabilities* $F_{mm'}$ $R_{mm'}$, $S_{Rmm'}$, and $S_{Lmm'}$ depend only on the relative orientation of the outgoing and incoming arms of the junction. The probability *amplitudes* $f_{mm'}$, $r_{mm'}$, $s_{Rmm'}$ and $s_{Lmm'}$ almost have this property: as may be calculated, they acquire also, however, extra phases $(-1)^{m-1}$ according to the scheme listed in Table I.

The circuit shown in Fig. 5(a) consists of two four-terminal junctions, whose centers are a distance $d$ apart. If we locate the origin of coordinates at the center of the left-hand side junction, all of our previous wave functions apply without any modification to that square and its sur-

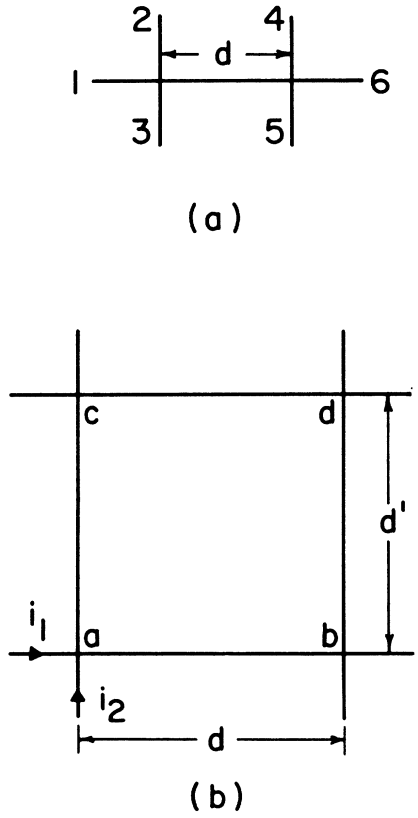


FIG. 5. More complicated junctions obtained by concatenation of the basic four-point junction: (a) the six-point junction, with a separation between centers of $d$; (b) the loop, a rectangle $d\times d'$. The notation is described in the text.

rounding arms. For the right-hand side junction, we proceed as follows: our previous solutions apply to any junction for which the zero of $\mathbf{A}$ is located at its center. If we now suppose that center to be at $(d,0,0)$, then our previous solution, with $x \to x-d, y \to y$ refers to the vector potential $\mathbf{A}'=(-By/2, B(x-d)/2, 0)$. The gauge transformation $\Lambda = Byd/2$, which brings us back to $\mathbf{A}=(-By/2, Bx/2, 0)$, together with the translation, produce in arms 1′ and 2′ of the right-hand side junction [in fact, the central arm and that labeled 4 in Fig. 5 (a)], for example, the wave functions

$$\psi_{1'}(x,y)=e^{ixy/2l^2}\sum_m [\alpha_m e^{ip_m d} e^{-ip_m x} f_m(y) + \alpha'_m e^{-ip_m d} e^{ip_m x} f_{-m}(y)] , \quad (3.1a)$$

$$\psi_{2'}(x,y)=e^{iyd/l^2} e^{-ixy/2l^2} \sum_m \gamma_m e^{ip_m y} f_m(x-d) . \quad (3.1b)$$

Comparing with Eqs. (2.15) and (2.17), we see that the total effect of the $x$ translation is to insert expected subband-dependent phase factors $e^{\pm ip_m d}$ in the horizontal arms and an overall subband-independent phase factor in the vertical arms. (Note that $d$ is the distance between *centers* of the junctions.)

This result allows us to develop the simple iterative scheme of the next section, in which we need go back no further than the amplitudes $r_{m'm}$, $f_{m'm}$, $s_{Rm'm}$, and $s_{Lm'm}$, with phase factors $q_m=(-1)^{m-1}$ and $e^{ip_m d}$ where appropriate, in order to calculate the properties of any collinear circuit.

We also wish to consider compound circuits that contain loops. The simplest such circuit is the rectangle shown in Fig. 5(b), made up of four, four-terminal junctions. A translation in the $y$ direction to $(0,d',0)$, accomplished in a manner similar to the $x$ translation just discussed, needs the gauge transformation $\Lambda'=-Bd'x/2$. The resulting functions, for the junction at $(0,d',0)$ but with vector potential $\mathbf{A}=(-By/2, Bx/2, 0)$, are

$$\psi_{1''}(x,y)=e^{-id'x/l^2} e^{ixy/2l^2} \sum_m [\alpha_m e^{-ip_m x} f_m(y-d') + \alpha'_m e^{ip_m x} f_{-m}(y-d')] , \quad (3.2a)$$

$$\psi_{2''}(x,y)=e^{-ixy/2l^2} \sum_m \gamma_m e^{-ip_m d'} e^{ip_m y} f_m(x) , \quad (3.2b)$$

where 1″ and 2″ refer to the left-hand side arm and upper arm of the upper left junction in Fig. 5(b). To construct wave functions for the top right-hand side junction, centered at $(d,d',0)$, we may take the functions constructed for the junction at $(d,0,0)$ and translate them upwards by $d'$. To repair the vector potential we need the same gauge transformation $\Lambda'$ as we just used. The net result, for functions centered on this junction but with $A=(-By/2, Bx/2, 0)$, is

$$\psi_{1'''}(x,y)=e^{-id'x/l^2} e^{ixy/2l^2} \sum_m [\alpha_m e^{ip_m d} e^{-ip_m x} f_{-m}(y-d') + \alpha'_m e^{-ip_m d} e^{ip_m x} f_m(y-d')] , \quad (3.3a)$$

$$\psi_{2'''}(x,y)=e^{-idd'/l^2} e^{idy/l^2} e^{-ixy/2l^2} \sum_m \gamma_m e^{-ip_m d'} e^{ip_m y} f_m(x-d) . \quad (3.3b)$$

An effect of the two successive gauge transformations is the appearance in $\psi_{2'''}$ of the inverse of the Aharonov-Bohm phase factor $\phi_{AB}=e^{idd'/l^2}$

It would be possible to obtain wave functions to describe this junction by performing the $x$ and $y$ translations in the opposite order. One then obtains expressions that are different from those we just derived [Eq. (3.3)] by a factor $\phi_{AB}$ in both arms. The appearance of the phase factor $\phi_{AB}$ depends on the path taken along the circuit to get to the junction, an expected property for such transformations. The total wave function of all four junctions, which we describe in a later section, will be a single-valued quantity, of course.

### C. An iterative scheme for multiterminal junctions

Once the scattering amplitudes have been calculated for the four-terminal junction, it is possible to combine these amplitudes iteratively for two or more four-terminal junctions so as to obtain amplitudes for multiterminal junctions. This is important since the experimental arrangements for the study of the Hall effect usually involve such multiterminal configurations.

First, we consider the combination of several four-terminal junctions so as to obtain a linear array of $n$ equally spaced junctions as pictured in Fig. 6(a). In the symbol $S^n_{ji}$ for the scattering amplitude for this $n$-terminal junction $i$ designates the arm through which the particles enter and $j$ the arm through which they leave, according to the numbering scheme in Fig. 6(a). In addition $S^n_{ji}$ is a matrix $S^n_{ji}(jm,im)$ in the space of modes (subbands), $im$ for the entrance arm and $jm$ for the exit arm. The indices $im$ and $jm$ are suppressed in the following discussion: the equations are matrix equations with matrix products and matrix inverses in this subband space. It is important that matrix products in these equations contain sums over the evanescent modes as well as the propagating modes for intermediate states, although the final products need only be evaluated with initial and final propagating modes in the external arms. We build up the scattering amplitude $S^n_{ji}$ from the basic $S^4_{ji}$ for the

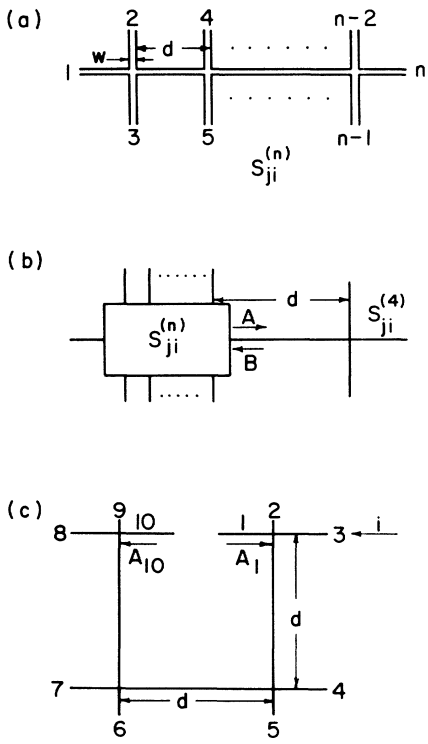


FIG. 6. Schematic representations, with appropriate notation (see text) for (a) the $n$-terminal junction; (b) the concatenation of it with the four-terminal junction to form the $(n+2)$-terminal junction; (c) the combination of four, four-terminal junctions just before closing to form the rectangular loop. The currents $A_{10}$, $A_1$, and $i$ are defined in the text.

four-terminal junction. These latter quantities can be obtained from $S_{j1}^4$, in which the entrance arm is 1, by suitable rotations, taking proper care of the phase factors of Table I that arise when the wave functions, of which the $S_{ji}^4$ are coefficients, are rotated. Another quantity that is needed is the diagonal matrix of propagators

$$P=e^{ip_{im}d} . \tag{3.4}$$

This describes the propagation of the plane waves with wave numbers $p_{im}$ depending on the mode (subband) numbers $im$. The distance $d$ is the distance between junction centers along the linear array of Fig. 6(a). Note that for the evanescent waves $p_{im}$ will have an imaginary part, describing the exponential decay of these modes as a function of distance away from a four-terminal junction; for $d$ sufficiently large, of course, the evanescent waves will have effectively decayed away at the next terminal.

Figure 6(b) illustrates how the $(n+2)$-terminal amplitude $S_{ji}^{n+2}$ is obtained by combining the four-terminal junction $S_{ji}^4$ on the right with the $n$-terminal junction $S_{ji}^n$ on the left. The derivation depends on the linearity of the problem and the definition of $S_{ji}^n$. With ingoing waves in several arms $i$ with amplitudes $a_i$, the outgoing waves in the arms $j$ will be given by linear combinations $\sum_i S_{ji}^n a_i$. We introduce the state vectors $A$ and $B$ describing the waves traveling to right and left in the wire connecting $S_{ji}^n$ and $S_{ji}^4$. $A$ and $B$ are column vectors in the subband space. They are meant to be the coefficients of the wave functions just to the right of $S_{ji}^n$. To propagate $A$ over to the place where these waves enter the four-terminal junction we need the product $PA$ of $A$ with the diagonal propagation matrix $P$ (3.4) [compare Eq. (3.1)]. Here and below we start with the initial state on the right and multiply on the left to obtain the final or intermediate states. Suppose now that the entrance arm for the $n+2$ terminal junction is one of the terminals $i<n$ of the $n$-terminal junction described by $S_{ji}^n$. We can calculate $B$ from $A$ using the properties of $S_{ji}^4$ and the propagation matrix $P$:

$$B=PS_{11}^4PA ; \tag{3.5}$$

i.e., propagate $A$ to the right with $P$, reflect it on the four-terminal junction and then propagate it back to the $n$-terminal junction. The $A$ has two sources, the entrance arm just alluded to and the wave $B$;

$$\begin{aligned} A&=S_{ni}^n+S_{nn}^nB \\ &=S_{ni}^n+S_{nn}^nPS_{11}^4PA . \end{aligned} \tag{3.6}$$

This matrix equation is easily solved:

$$A=(1-S_{nn}^nPS_{11}^4P)^{-1}S_{ni}^n . \tag{3.7}$$

Once we know $A$ and consequently $B$ from (3.5), we can find the desired $n+2$-terminal scattering amplitudes. If the exit channel $j<n$ is attached to the $n$-terminal junction on the left (recall $i<n$ also),

$$S_{ji}^{n+2}=S_{ji}^n+S_{jn}^nB, \quad (j<n) . \tag{3.8}$$

If the exit channel $j$ is attached to the four-terminal junction on the right,

$$S_{ji}^{n+2}=S_{j-n+2,1}^4PA, \quad (j\geq n) . \tag{3.9}$$

This takes care of the cases $i<n$. For the cases $i=n$, $n+1$, and $n+2$, where the entrance arm is one of the terminals of the four-terminal junction on the right we have to proceed differently. In the present case of a linear $n+2$-terminal junction we can obtain these cases by rotation through 180°, starting with one of the cases $i<n$, paying careful attention to phase factors. If this were not available, as in the case described below of terminals arranged in a square, we would need to derive equations similar to but slightly different from (3.5)–(3.9) with the entrance channel on the four-terminal junction on the right.

Once the scattering amplitudes are known, the remainder of the calculation, leading to the voltages at the various terminals for specified currents, the Hall resistance, etc., is done in terms of amplitudes squared and summed over the open channels (i.e., those with propagating modes)

$$T_{ji}=\sum_{\substack{im,jm \\ \text{open}}} |S_{ji}(jm,im)|^2 . \tag{3.10}$$

Before proceeding we note that unitarity (conservation of probability) demands

$$\sum_j T_{ji} = n_0 \ , \tag{3.11}$$

where $n_0$ is the number of open channels. Further, reciprocity (time-reversal invariance) gives $T_{ji}(\mathbf{B}) = T_{ij}(-\mathbf{B})$, where $\mathbf{B}$ is the magnetic field. Since the system with magnetic field reversed is also a possible system, we find

$$\sum_i T_{ji} = n_0 \ , \tag{3.12}$$

where the sum is now over the incident arms. The conditions (3.11) and (3.12) are very useful checks on the computer code.

To proceed further we use the formalism of Büttiker.[8] The conductance matrix in units of $e^2/h$ is

$$\sigma_{ji} = n_0 \delta_{ji} - T_{ji} \ . \tag{3.13}$$

The currents entering the terminals $I_j$ are related to the voltages on the terminals $V_i$ by

$$I_j = \sum_{i=1}^{N_l} \sigma_{ji} V_i, \quad (j = 1,2,\ldots,N_l) \ . \tag{3.14}$$

Although $i$ and $j$ range from 1 to the number of legs $N_l$, the $I_j$ are not independent [$\sum_{j=1}^{N_l} I_j = 0$, see Eq. (3.11)], and, furthermore, we can add the same voltage $V$ to all the $V_i$ without changing the currents [see Eq. (3.12)]. We consider the special case with the currents $I_1 = -I_{N_l}$ and all other currents zero, and we take $V_{N_l} = 0$, thus truncating the matrix equation (3.11) to a space of dimension $N_l - 1$, with $I_j = (1,0,0,\ldots,0)$. In this space the matrix $\sigma_{ji}$ is nonsingular and we can invert to solve (3.14) for the $V_i$ corresponding to unit current from arm 1 to arm $N_l$. Differences of these $V_i$ give the components of the resistance matrix in units of $h/e^2$. Numerical results will be given in Sec. IV.

### D. Loop circuit

The formalism described above is readily modified to describe an array of terminals arranged around a square—see Fig. 6(c). Two new features appear when we complete the square, i.e., join arm 1 to arm 10. These describe the manifestation of the Aharonov-Bohm effect in our formalism.

First, there are the phase factors associated with the necessity of doing the calculation with the same unique choice of gauge for all the various junctions of Fig. 6(a) or 6(c) displaced from each other by translations $d$ in the $x$ or $y$ directions. These were discussed in Sec. III B. A translation in the $x$ direction by a distance $d$ is described by Eqs. (3.1a) and (3.1b). For the linear array of Fig. 6(a) the factors $e^{\pm i p_m d}$ are properly included in our phase matrix $P$, Eq. (3.4) and the factor $e^{iyd/l^2}$ in (3.1b) drops out when the amplitudes are squared. However, for the square of Fig. 6(c) the situation is more complicated. When we make four successive translations $(x \to x-d, y \to y)$, $(x \to x, y \to y+d)$, $(x \to x+d, y \to y)$, and $(x \to x, y \to y-d)$, around the square of Fig. 6(c) and the four concomitant gauge transformations necessary to keep the gauge always the same $\mathbf{A} = (-By/2, Bx/2, 0)$ with $x = y = 0$ the origin of the first junction, the wave functions change to

$$\psi_1'''' = \phi_{AB} \psi_1 \ , \qquad \psi_2'''' = \phi_{AB} \psi_2 \ , \tag{3.15}$$

where $\phi_{AB} = e^{id^2/l^2}$. Thus wave functions for all arms of a single four-terminal junction pick up the Aharonov-Bohm phase factor after one loop of transformation as noted in the last paragraph of Sec. III B.

In addition, when we join arm 10 to arm 1 in Fig. 6(c) to form a square circuit enclosing the flux $Bd^2$, we have an additional set of self-consistency conditions to satisfy. Suppose $A_1$ and $A_{10}$ are the state vectors describing the total ingoing currents in wires 1 and 10 to the neighboring four-terminal junctions. In addition we have an ingoing current in arm $i$ [arm 3 in Fig. 6(c)]. We designate by $S_{ji} \equiv S_{ji}^{10}$ the scattering matrix for the square array of Fig. 6(c) before joining. This is obtained from equations like those for the linear array described above, with the modifications due to the square geometry. After joining wires 1 and 10 we have three source currents $i$, $A_1$ and $A_{10}$, so using linearity to find the total right and left currents in the joined wire, also $A_1$ and $A_{10}$, we find the self-consistency conditions

$$\begin{aligned} \phi_{AB} A_1 &= PS_{10,i} + PS_{10,1} A_1 + PS_{10,10} A_{10} \ , \\ \phi_{AB}^{-1} A_{10} &= PS_{1,i} + PS_{1,1} A_1 + PS_{1,10} A_{10} \ . \end{aligned} \tag{3.16}$$

The phase factors on the left compensate for the Aharonov-Bohm phases in (3.15). Once we have solved (3.16) for $A_1, A_{10}$ we calculate the outgoing amplitude in arm $j$ as before to obtain the scattering amplitudes for the square:

$$S_{ji}^{\square} = S_{ji} + S_{j,1} A_1 + S_{j,10} A_{10}, \quad i = 2,3,\ldots,9 \ ; \quad j = 2,3,\ldots,9 \ . \tag{3.17}$$

### E. Alternative method for the loop circuit

An alternative view of the loop circuit allows one to see some of its symmetry properties. For brevity we specialize to the square loop circuit shown in Fig. 5(b) with $d = d'$. Symmetry allows us to restrict our attention to only two incident waves, $i1$ or $i2$. We have already developed in Sec. II the wave functions appropriate to each of the four, four-terminal vertices. For those vertices without external currents there are only two separate orientations of these wave functions needed, corresponding in each case to incident waves along one of the connecting arms. At the lower left junction there are three sets of four-terminal wave functions, two associated with incident waves in the two connecting arms and one for the incident wave $i1$ or $i2$. Along each arm, there is a two-component equation relating the amplitudes of waves traveling in each of two directions. For example, denoting the amplitudes of the incident clockwise (counterclockwise) waves at each vertex by $A_\alpha^{cw}$ ($A_\alpha^{ccw}$), where $\alpha = a,b,c,d$ refers to the vertices as in Fig. 5(b), the equa-

tions for the arm connecting vertices $c$ and $d$, are

$$R A_d^{\rm cw}+S_L A_d^{\rm ccw}=A_c^{\rm ccw} ,$$
$$A_d^{\rm cw}=S_R A_c^{\rm cw}+R A_c^{\rm ccw} , \tag{3.18}$$

where $R$, $S_R$, and $S_L$ are $M\times M$ matrices whose elements are, respectively, $e^{ip_m d}q_m r_{mm'}$, $e^{ip_m d}s_{R,mm'}$, and $e^{ip_m d}q_m s_{L,mm'}$. For the arms joining at vertex $a$ the equations for the clockwise and counterclockwise amplitudes also involve the amplitudes of the incident external wave, $A_{i1}$ or $A_{i2}$. These eight equations can be written in a compact two-component notation using vectors

$$\Psi_\alpha=\begin{bmatrix} A_\alpha^{\rm cw} \\ A_\alpha^{\rm ccw} \end{bmatrix}, \quad \alpha=a,b,c,d , \tag{3.19}$$

and matrices

$$\mathcal{L}=\begin{bmatrix} R & S_L \\ 1 & 0 \end{bmatrix}, \quad \mathcal{R}=\begin{bmatrix} 0 & 1 \\ S_R & R \end{bmatrix} , \tag{3.20}$$

where $R$, $S_L$, and $S_R$ are the same matrices as in Eq. (3.18). The eight equations become

$$\mathcal{L}\psi_a-\phi_{\rm AB}^{-1}\mathcal{R}\psi_b=\psi_{i,u} ,$$
$$\mathcal{L}\psi_c-\mathcal{R}\psi_a=\psi_{i,1} ,$$
$$\mathcal{L}\psi_b-\mathcal{R}\psi_d=0 , \tag{3.21}$$
$$\mathcal{L}\psi_d-\mathcal{R}\psi_c=0 .$$

The incident spinors are given by

$$\psi_{i,u}=\begin{bmatrix} -FA_{i1}-S_R A_{i2} \\ 0 \end{bmatrix}, \quad \psi_{i,1}=\begin{bmatrix} 0 \\ S_L A_{i1}+FA_{i2} \end{bmatrix} , \tag{3.22}$$

where $F$ is the $M\times M$ matrix $e^{ip_m d}q_m f_{mm'}$. With our particular choice of wave functions, as described in Sec. III B, the Aharonov-Bohm phase $\phi_{\rm AB}=e^{id^2/l^2}$ appears only in the first equation.

These matrix equations can be solved in a standard way, so that for example

$$\psi_a=[1-\phi_{\rm AB}^{-1}(\mathcal{L}^{-1}\mathcal{R})^4]^{-1} \times[\mathcal{L}^{-1}\psi_{i,u}+\phi_{\rm AB}^{-1}(\mathcal{L}^{-1}\mathcal{R})^3\mathcal{L}^{-1}\psi_{i,1}] . \tag{3.23}$$

With this closed expression, one can foresee the possibility of large internal amplitudes, depending on the size of the factor in the first set of square brackets. This factor would be zero, making the amplitude $\psi_a$ infinite, if one of the eigenvalues of $(\mathcal{L}^{-1}\mathcal{R})^4$ was equal to $\phi_{\rm AB}$, which would occur if an eigenvalue of $\mathcal{L}^{-1}\mathcal{R}$ is equal to $\lambda\phi_{\rm AB}^{1/4}$, where $\lambda^4=1$, or $\lambda=1,i,-1$ or $-i$. An actual zero will occur only for unphysical, complex values of $kw$, but, for real $kw$, the factor can pass close to zero, a behavior characteristic of resonant scattering. We can anticipate that such resonances should show up in the voltages on the external leads. The approximate four fold symmetry in the circuit, due to its shape, resembles, but is quite distinct from, the symmetry of the resonant states of the four-point junction discussed earlier.

## IV. RESULTS

### A. Hall resistance of the four-terminal junction

The general analysis of Büttiker[8] gives the Hall resistance $R_H$ as a function of the total probabilities discussed at the end of Sec. II D, $F=\sum_{nn'}F_{nn'}$, $S_R=\sum_{nn'}S_{Rnn'}$, $S_L=\sum_{nn'}S_{Lnn'}$, and $R=\sum_{nn'}R_{nn'}$, summed over all open channels:

$$\mathcal{R}=\frac{e^2}{h}R_H=\frac{2(S_R-S_L)}{(2F+S_R+S_L)^2+(S_R-S_L)^2} . \tag{4.1}$$

It is noteworthy that the unitarity property, which limits the total quantities by $R+F+S_R+S_L=n_0$, does not restrict $\mathcal{R}$ to be $1/n_0$, the expected large-$w$ result. The plateau with this value of $\mathcal{R}$ corresponds to $S_R=n_0$ and all the other probabilities being zero, but unitarity certainly does not require those values. For physically accessible values of the scattering probabilities, $\mathcal{R}$ may be larger or smaller than $1/n_0$, and it may even be negative (see also Ref. 15). These departures are the consequence of quantum effects associated with the junction, and they constitute the new results that we present.

In Fig. 7 we show three-dimensional graphs of the results of our calculation, the surface $\mathcal{R}$ as a function of $kw$ and $\mathcal{B}=w^2/l^2=(w^2q/\hbar c)B$. Figure 7(a) gives a slightly different perspective on the same results presented in Fig. 2 of our previous publication.[10] The wide wire integer quantum Hall effect can be seen in the large $w^2/l^2=\mathcal{B}$ portion of the graph, where the wire width $w$ is large compared with the magnetic length $l$. In this region, we find $S_R=n_0$, and thus $\mathcal{R}=1/n_0$, except at the abrupt transitions, where $n_0$ changes as a new propagation mode opens. Figure 7(b) is a head-on view looking along the $B$ axis. Figure 7(c) gives a close-up view of the complicated behavior near $kw=6.0$ and $\mathcal{B}\le 10.0$. In Fig. 8 we show three slices at fixed $kw$ through this region and in Fig. 9 two slices at fixed $B$. We note in particular the quenching[1] of the Hall resistance at small $B$ for the special value $kw=5.5$ shown in Fig. 8(a) and the extra plateau (which is not at $1/n_0$) in Fig. 8(c).

#### 1. Phase-shift analysis

We have attempted to understand the structure in these results in terms of the predominant influence of states with specific quantum numbers. The quantum numbers depend on the symmetry of the system together with its boundary conditions. For any value of $\mathcal{B}$, even with the walls in place, the four terminal junction is invariant with respect to rotations through $\pi/2, R(\pi/2)$, in the plane of the junction. Since four such rotations in sequence produce the identity operation, states can be classified into four symmetry classes such that

$$R(\pi/2)\psi(x,y)=\psi(y,-x)=\lambda\psi(x,y) , \tag{4.2}$$

with $\lambda^4=1$, i.e.,

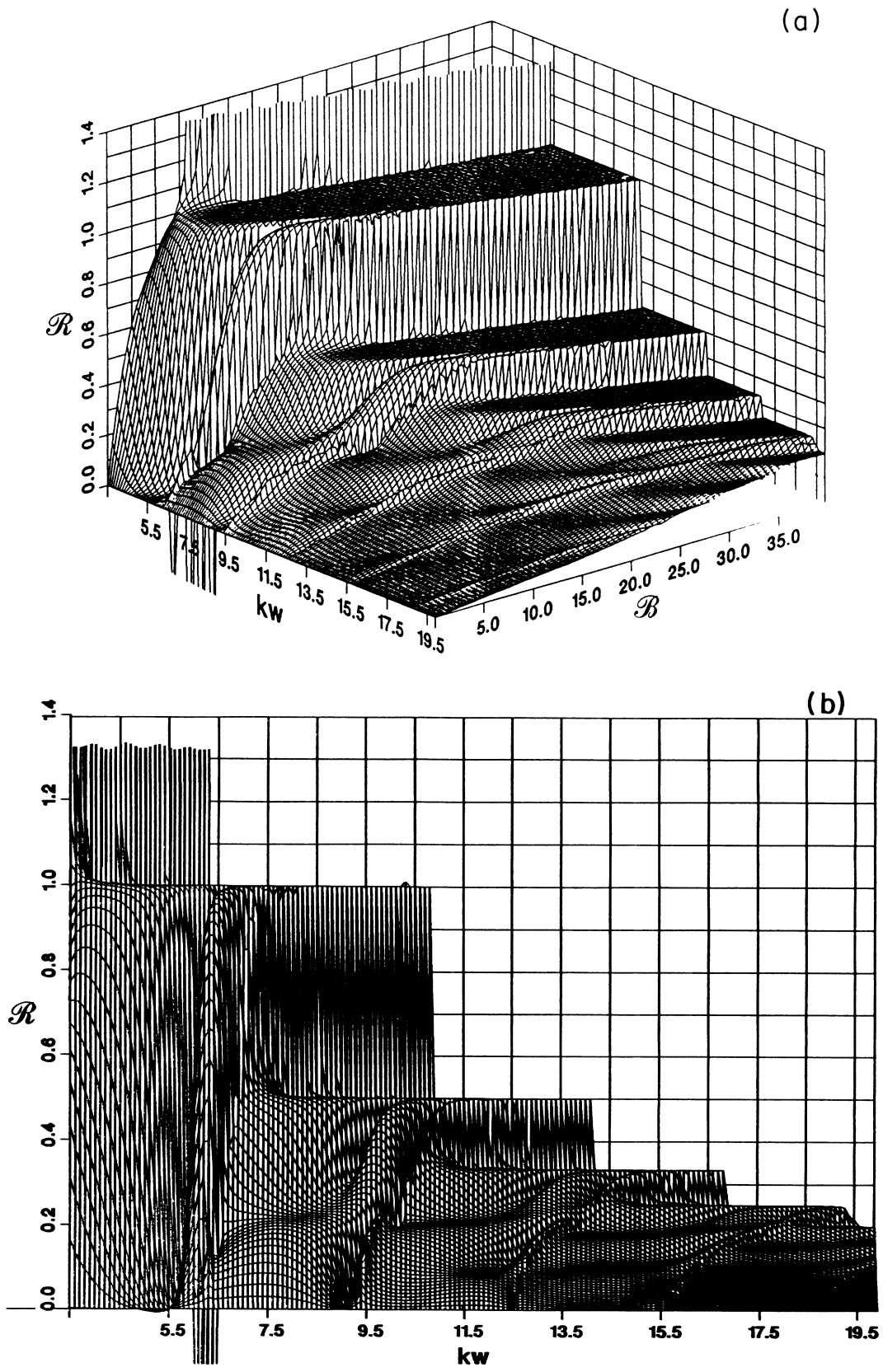


FIG. 7. Three-dimensional representations of the Hall resistance of a four-terminal junction as a function of the dimensionless energy quantity $kw$ and the dimensionless magnetic field $\mathcal{B}$, (a) in oblique view; (b) along the $\mathcal{B}$ axis; (c) in detail for the region near the second band edge.

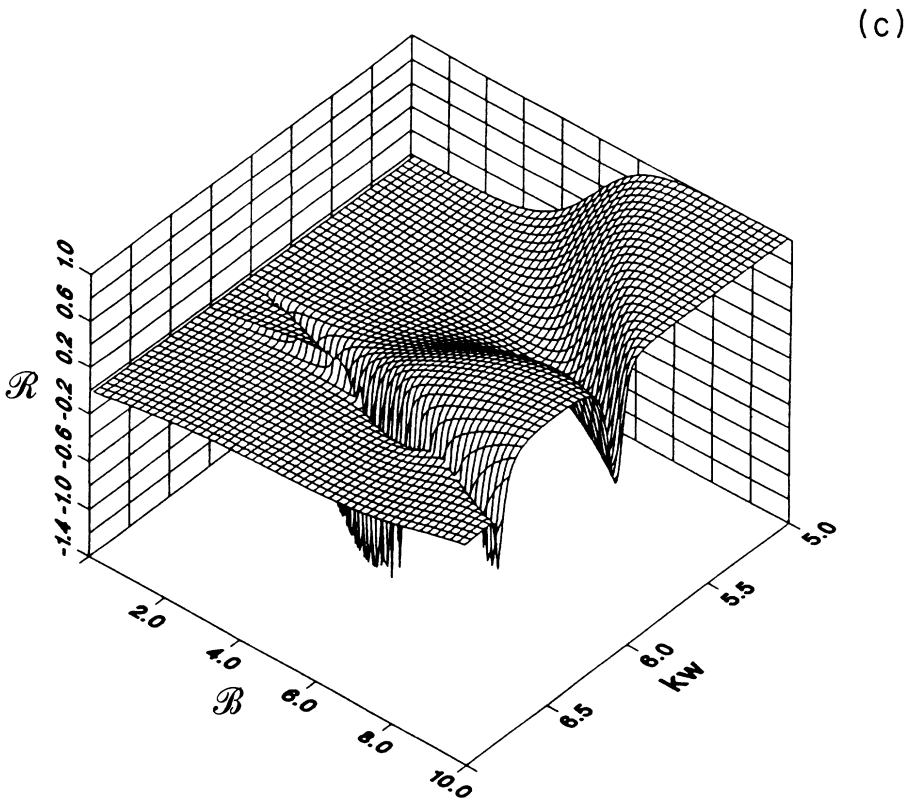


FIG. 7. (*Continued*).

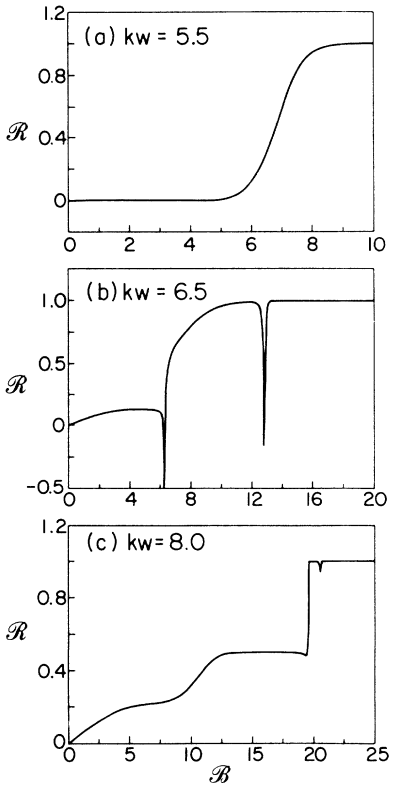


FIG. 8. For the four-terminal junction, sections through the $\mathcal{R}$ surface shown in Fig. 7: a range of $\mathcal{B}$ (a) at $kw=5.5$, below the second band edge; (b) at $kw=6.5$, showing structure at the second band edge; (c) at $kw=8.0$.

$$\lambda=1,-1,i,-i\ . \tag{4.3}$$

For each of these four states the wave functions in the four arms differ only by powers $\lambda^n$, $n=1,4$, of these four values of $\lambda$. The amplitudes in the four arms for each of the four states (the arm numbers refer to Fig. 1) are shown in Table II.

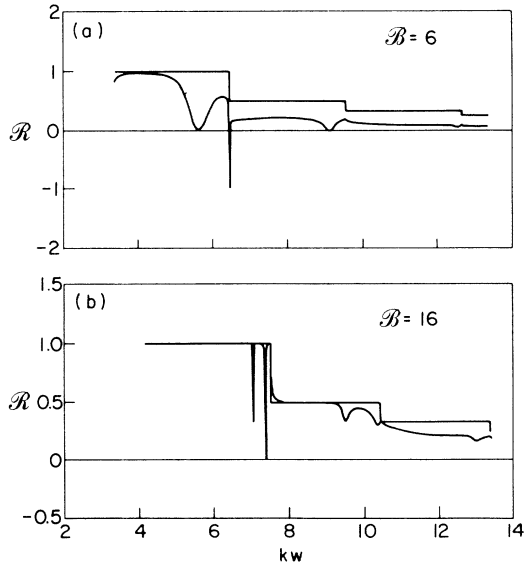


FIG. 9. Additional sections through the $\mathcal{R}$ surface of Fig. 7: a range of $kw$ values for (a) $\mathcal{B}=6.0$ and (b) $\mathcal{B}=16.0$. Also shown is the quantity $1/n_0$, where $n_0$ is the number of open channels.

TABLE II. Relative phases of wave functions in the arms of the four-terminal junction, corresponding to the states $\lambda$, Eq. (4.3).

| $\lambda$ \ arm | 1 | 3 | 4 | 2 |
|---|---|---|---|---|
| 1 | 1 | 1 | 1 | 1 |
| $-1$ | 1 | $-1$ | 1 | $-1$ |
| $i$ | 1 | $i$ | $-1$ | $-i$ |
| $-i$ | 1 | $-i$ | $-1$ | $i$ |

In terms of the states designated by $\lambda$ the scattering amplitudes $S_\lambda$ for the four-terminal junction are diagonal in $\lambda$. $S_\lambda$ is still a matrix in subband $m,m'$ space. Referring to Table II we find the amplitudes for reflection, forward scattering, and scattering to the right and left

$$\begin{aligned} r &= \tfrac{1}{4}(S_1+S_{-1}+S_i+S_{-i}) , \\ f &= \tfrac{1}{4}(S_1+S_{-1}-S_i-S_{-i}) , \\ s_r &= \tfrac{1}{4}(S_1-S_{-1}+iS_i-iS_{-i}) , \\ s_l &= \tfrac{1}{4}(S_1-S_{-1}-iS_i+iS_{-i}) . \end{aligned} \tag{4.4}$$

Inverting these equations we find the amplitudes $S_\lambda$:

$$\begin{aligned} S_1 &= r+f+s_r+s_l , \\ S_{-1} &= r+f-s_r-s_l , \\ S_i &= r-f-is_r+is_l , \\ S_{-i} &= r-f+is_r-is_l . \end{aligned} \tag{4.5}$$

For wave numbers $kw$ such that only one channel ($m$ valve of Sec. II A) is open the amplitudes $S_\lambda$ can be written in terms of real phase shifts $\delta_\lambda$,

$$S_\lambda = e^{2i\delta_\lambda} . \tag{4.6}$$

For higher wave numbers with several open channels we have only the weaker unitarity requirement

$$|S_\lambda| \le 1 , \tag{4.7}$$

since the incoming wave is in one channel, but the outgoing wave is partly transferred to other channels (different $m$ values).

We can obtain information about the states responsible for the structures evident in Fig. 7 by performing a "phase-shift analysis" of the sort just discussed. From the amplitudes $r,f,s_r,s_l$ used to calculate the Hall resistance we can calculate the amplitudes $S_\lambda$ from Eq. (4.5) and from these the phase shifts using Eq. (4.6) for $kw$ below the second threshold. Phase shifts calculated in this way and the corresponding Hall resistance for the three values $B=2.0,8.0,16.0$ are given in Fig. 10. It is easy to identify pronounced drops in the Hall resistance with resonant behavior, i.e., rapid increase of the phase shift through $\pi$, in states with specific $\lambda$ values. At $\mathcal{B}=2.0$ resonant behavior in the $\lambda=-1$ state corresponds to a dip in $\mathcal{R}$ at $kw\simeq 6.1$. At $\mathcal{B}=8.0$ resonant behavior in the $\lambda=-i$ state corresponds to a dip in $\mathcal{R}$ at $kw\simeq 5.8$. At $\mathcal{B}=16.0$ we have two dips in $\mathcal{R}$ corresponding to states with $\lambda=-i$ and $\lambda=1$.

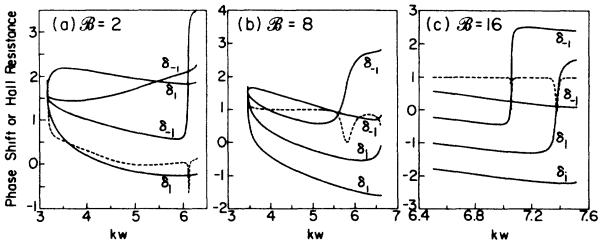


FIG. 10. Phase shifts for the four states with $\lambda$ symmetry (full lines) and the Hall resistance (dashed line) for the four-terminal junction over the range of values of $kw$ below the second band edge; (a) for $\mathcal{B}=2.0$; (b) for $\mathcal{B}=8.0$; (c) for $\mathcal{B}=16.0$.

For $\mathcal{B}=8.0$ the second threshold is at $kw\simeq 6.6$. For larger $kw$ the phase shifts $S_\lambda$ become complex. In this range of $kw$ we can still obtain the amplitudes $S_\lambda$ from Eq. (4.5). To display them graphically we give in Fig. 11 Argand plots, i.e., plots of $\mathrm{Im}S_\lambda$ versus $\mathrm{Re}S_\lambda$ as functions of $kw$. The unitarity condition constrains these plots to the interior of the unit circle, and below the second threshold the plot will lie on the unit circle. Resonant behavior appears in such an Argand plot as rapid (as a function of $kw$) traversal of a circle (of radius $\le 1$) in the counterclockwise sense with increasing $kw$. The circle (of unit radius) corresponding to the $\lambda=-i$ state at $kw\simeq 5.8$

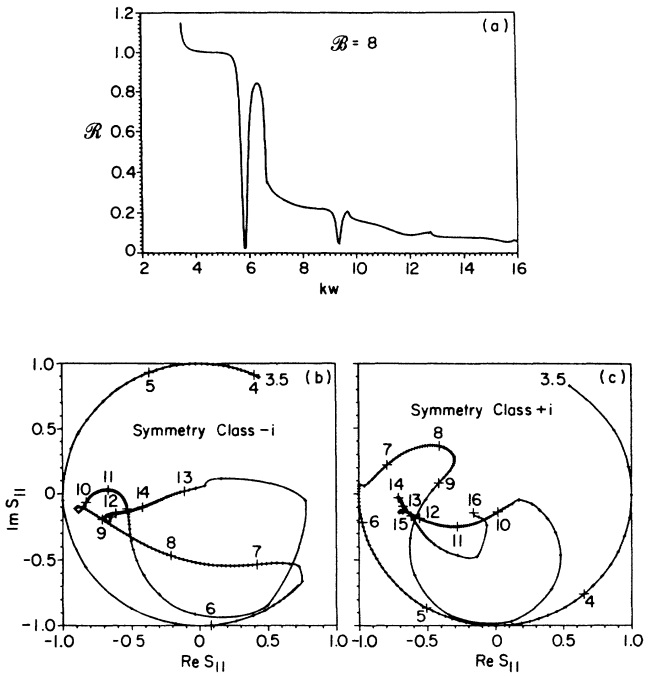


FIG. 11. For the four-terminal junction at $\mathcal{B}=8.0$: (a) structure of the Hall resistance as a function of $kw$; (b) Argand diagram of the scattering amplitude for the particular scattering state of symmetry class $\lambda=-i$ responsible for the rapid variation of $\mathcal{R}$ near $kw=5.8$; and (c) Argand diagram for the state with $\lambda=i$, associated with the dip at $kw=9.4$.

below the second threshold is evident in Fig. 11(b). It is also easy to identify a circular pattern in Fig. 11(c) for the $\lambda=i$ state and associate it with the rapid dip in the Hall resistance at $kw=9.6$. In this way we can find quantum numbers for the states responsible for the principle structures in the Hall resistance of Fig. 11(a).

Rapidly varying phase shifts for real $kw$ generally signify the presence of a pole of the scattering matrix at a nearby complex value of $kw$. For our problem the scattering matrix is the inverse of the matrix appearing on the left side of Eq. (2.20). The poles of the scattering matrix thus correspond to the zeros of the determinant of the matrix of Eq. (2.20). We can search for these zeros with a Newton's method using solutions of the differential equations for complex $kw$. This has proved to be a more efficient way than the phase-shift analysis for identifying states corresponding to important structures in the Hall resistance, and we now describe some of the results.

### 2. *Resonant states as poles of the scattering matrix: real and virtual levels*

As with any scattering problem, rapid variations in the partial cross sections (probabilities $F$, $S_R$, and $S_L$) may be associated with virtual levels (resonant states) of the system. To enumerate the possibilities for our system, whose properties depend on the strength of the magnetic field, we recall that for $\mathcal{B}=0$ there are two bound states, the ground state at $kw\simeq 2.56$, which has even parities in both the $x$ and the $y$ directions, and the first excited state at $kw\simeq 6.06$, which has odd parities. At zero $\mathcal{B}$ we expect to find poles in our scattering matrix at these values of $kw$. At higher $\mathcal{B}$, these poles should persist, changing position smoothly as a function of $\mathcal{B}$, and carry some remnant of their zero-$\mathcal{B}$ symmetry.

Relevant to the high-$\mathcal{B}$ limit are the two-dimensional Landau orbits. They are the solutions for motion in a transverse magnetic field in a two-dimensional region of infinite extent. They have wave functions $\phi_{nm}(r,\theta)=\chi_{n|m|}(r)\exp(im\theta)$, where the function $\chi_{n|m|}(r)$ has $n-1$ radial nodes, and energy levels such that $(kw)^2=(2n-1+|m|-m)\mathcal{B}$. The levels possess discrete degeneracies, e.g., that for all $m\geq 0$. Physically the $m\leq 0$ wave functions correspond to positively charged particles moving in clockwise circles with energy levels given by the Landau formula. Out of them can be constructed wave packets representing the appropriate classical trajectories. The $m>0$ states have radial wave functions identical to those of the corresponding $m<0$ states, and their $\theta$ dependence appears to correspond to motion in a sense opposite to that of the classical motion. However, they cannot be used to construct wave packets of counterclockwise-rotating particles. For a given $n$, they have an expectation value for net kinetic angular momentum

$$\langle mrv_\theta\rangle=\left\langle\left[\mathbf{r}\times\left[\mathbf{p}-\frac{q}{c}\mathbf{A}\right]\right]_z\right\rangle=-\hbar(2n-1+|m|-m)\ ,$$

which is, for $m>0$, independent of the $m$ of the $\theta$ dependence, and is equal to that of the $m=0$ state. They are an infinite set, degenerate in energy and angular momentum, and their purpose is, by appropriate superposition with states of $m\leq 0$, to permit a translation of the center of the motion, a possibility that must exist in an infinitely extended $\mathcal{B}$ field. Since the classical turning point of the $n,m$ states is $r_t\sim 2(2n-1+|m|)^{1/2}l$, and our channels are only $w$ wide, the presence of poles corresponding to Landau levels of a given $n$ and $m$ must clearly depend on $l$ being small compared with $w$, i.e., on $\mathcal{B}=w^2/l^2$ being large. For $r_t/w$ much less than 1, we may expect to be able to identify the dominate $n,m$ values of our resonant states as the presence of the wall becomes less important. As we locate the poles corresponding to the various exact $\lambda$ symmetries, we will be able to identify them at large $\mathcal{B}$ with Landau orbitals of specific $n$ and $m$.

It is necessary to obtain the sets of solutions $f_m$ of the differential equations for complex values of $kw$. The poles are located by searching for the zeroes of the determinant of the matrix (2.20) as a function of complex $kw$ by using Newton's method. It is possible either to locate such a zero and to determine its $\lambda$ symmetry by examining the phase relationship of the wave functions in the four arms, or, more economically, to impose a particular $\lambda$ symmetry on the wave function and to look for zeros of a determinant of reduced size. When the poles correspond to decaying states, which is the case for all except those below the first band edge, $kw$ has a negative-imaginary part. Consequently, as may be verified from the zero-$\mathcal{B}$ relationship $(p_m w)^2=(kw)^2-(m\pi)^2$, the values of $p_m w$ for those channels that are open also have a negative-imaginary part. The $p_m w$ values for the closed channels are mainly positive imaginary, now with a small negative real part. As $\mathcal{B}$ is changed, the value of $\mathrm{Re}(kw)$ may approach a band edge $k_i w$. As $kw$ passes below $k_i w$ in the complex $kw$ plane, care must be taken in the calculation of $p_i w$ so that its complex phase increases in a continuous manner. In the computation, this necessitates the rotation of cuts of complex functions such as the square root.

The zero-$\mathcal{B}$ ground state possesses the exact rotation symmetry $\lambda=1$. Calculations show that it remains a stable state, below the first band edge for all $\mathcal{B}$. The modulus squared of its spatial wave function $\psi(x,y)$ is displayed in Fig. 12 for $\mathcal{B}=0$ and $\mathcal{B}=15$. There is evident contraction of the wave function due to the magnetic field. A property of all such exact states is that for general $\mathcal{B}$ they can be represented by a superposition of Landau levels with the same exact symmetry. In this case that symmetry is $\lambda=1$, so that the superposition can include all Landau levels with $m=4p$, where $p$ is a positive or negative integer. This admixture produces the indentations (with fourfold symmetry) of the wave function at $\mathcal{B}=15$, Fig. 12. As $\mathcal{B}$ increases further, the reduced spatial size of the motion (proportional to $l$) means that less of the admixture of higher Landau orbitals is needed. Thus as $\mathcal{B}$ tends to infinity, this state tends to the nodeless Landau level $n=1, m=0$. It is evident from Fig. 12, however, that $\mathcal{B}\leq 15$ is still somewhat distant from that limit. In the present noninteracting electron phase of our calculation this state has no effect on the Hall resistance

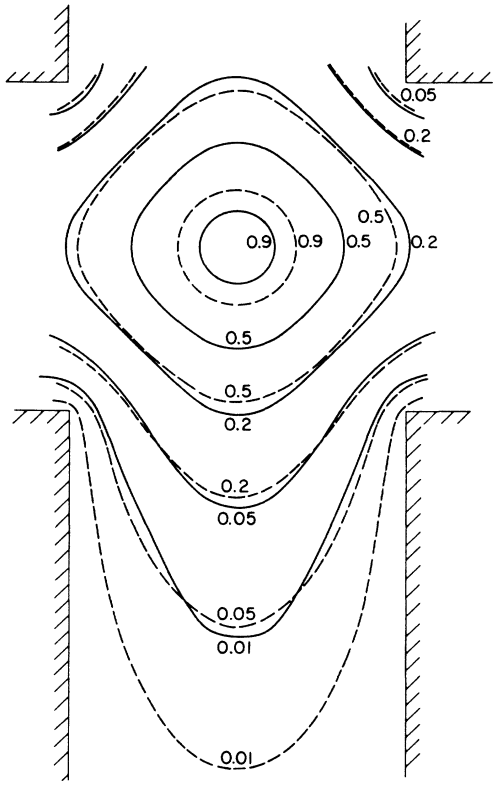


FIG. 12. Contour plots of $|\psi|^2$ of the bound state lying below the first band edge, for $\mathcal{B}=15$ (solid lines) and $\mathcal{B}=0$ (dashed lines).

$\mathcal{R}$.

The wave function of the zero-$\mathcal{B}$ first excited state has odd parity in both $x$ and $y$ directions, and has opposite signs on adjacent arms. It thus has the symmetry $\lambda=-1$. When $\mathcal{B}$ is not zero, parity is no longer conserved, and this state acquires a finite width, i.e, at the pole $kw$ has a negative-imaginary part. As $\mathcal{B}$ increases this width increases, and Re($kw$) grows faster than the $kw$ of the second band edge, which it crosses when $\mathcal{B}\sim 6$. The negative values of $\mathcal{R}$ at $kw\simeq 6.5$ for $\mathcal{B}=6$ are produced by this virtual state, which at that value of $\mathcal{B}$ occurs close to the second band edge. At $\mathcal{B}=8$ the pole $kw$ has crossed the band edge, and is on an unphysical sheet of the scattering matrix. As can be seen from Fig. 8(c) it no longer affects $\mathcal{R}$.

A finite value of $\mathcal{R}$ requires that left and right scattering have unequal probabilities, and thus must involve the states of $\lambda=i$ and $-i$ symmetry; conversely, a zero value of $\mathcal{R}$ requires that $\delta_i$ and $\delta_{-i}$ become equal (modulo $\pi$), which will happen when one of them changes rapidly by an amount comparable to $\pi$. The rapid variations of $\mathcal{R}$ that occur at the values $kw\simeq 5.8$ and 9.3 in Fig. 11(a) must therefore be associated with virtual states of one or the other of these symmetries. These states are found to have large widths as $\mathcal{B}$ tends to zero (and thus have little physical effect there) while as $\mathcal{B}$ increases they become narrower. Since from Fig. 11(b) the amplitude for the $\lambda=-i$ state goes rapidly through $-1$ at $kw\simeq 5.8$, it is predicted that $\lambda=-i$ is the symmetry character of the state involved, and pole position calculations confirm this prediction. For $\mathcal{B}$ large ($\sim 15$) the pole stays just below the second band edge to become the $n=1, m=-1$ Landau level. Similarly, from Fig. 11(c) we may deduce that the $kw\simeq 9.3$ structure is due to a $\lambda=i$ state. The pole approaches the third band edge as $\mathcal{B}$ increases, and crosses behind it (onto an unphysical sheet of the scattering matrix) at $\mathcal{B}\sim 13$. By then its wave function resembles that of the $n=1, m=1$ Landau level.

For the poles we have located, the real and imaginary parts of $kw$ are shown in Fig. 13 as functions of $\mathcal{B}$. The band edges and the Landau energies are also plotted there. As a consequence of the confining geometry, the

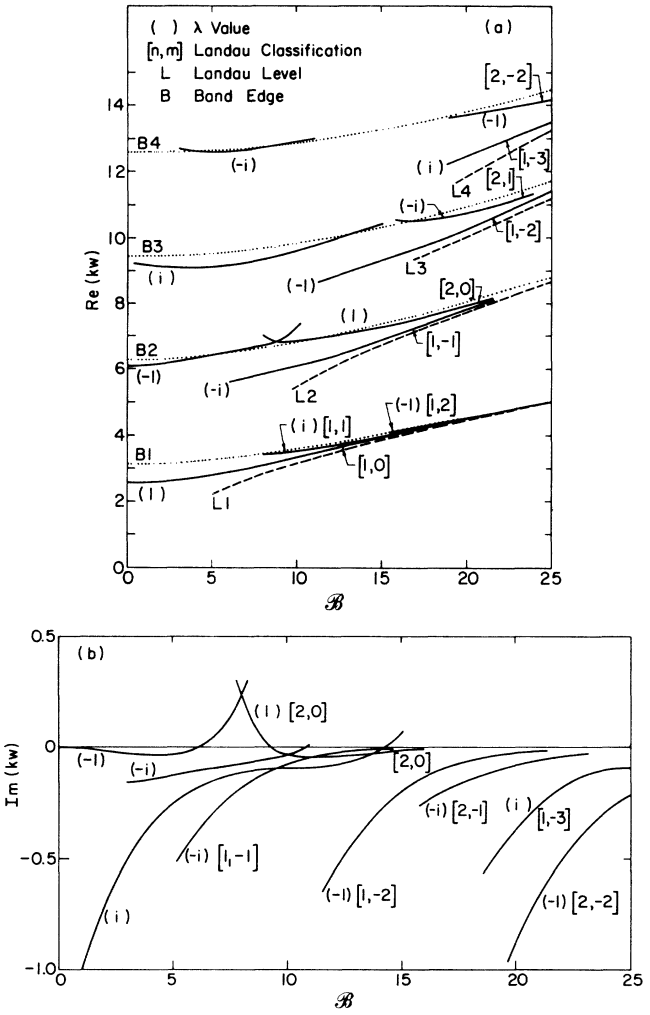


FIG. 13. Location of complex $kw$ for the bound and resonant states of the four-terminal junction, as a function of $\mathcal{B}$. (a) Re($kw$), solid lines. The dotted curves labeled $Bn$, $n=1,\ldots,4$ are the $kw$ values of the band edges, and the dashed curves $Ln$ are the Landau levels asymptotic to them at large $\mathcal{B}$. The $\lambda$ values of the exact fourfold rotation symmetry of the state are indicated by ($\lambda$), and the quantum numbers $n$, $m$ of the two-dimensional Landau levels to which the states are asymptotic in $\mathcal{B}$ are shown by $[n,m]$. (b) Im($kw$), solid lines. The notation for quantum numbers is as in (a).

band edges lie above the Landau levels and approach them as $\mathcal{B}$ increases. At $\mathcal{B}=20$, where $r_t/w \simeq 0.44$, the ground state, with $\lambda=1$, is just above the first Landau level. Above it but below the first band edge (i.e., on the physical sheet of $kw$) are successively the states $\lambda=i$, which we identify as $n=1, m=1$, and $\lambda=-1$, or $n=1, m=2$. There is no $\lambda=-i$ state there. At $\mathcal{B}=15$, the situation is almost the same, except that the last-mentioned ($\lambda=-1$) state has moved onto the second (unphysical) sheet. Just below the second band edge at $\mathcal{B}=20$, there is the first $\lambda=-i$ state, $n=1, m=-1$, and slightly above it another $\lambda=1$ state that we identify as $n=2, m=0$. We observe that this state is larger in physical extent than the $n=1, m=0$ state (the ground state), and that states with $\lambda=i$ and $-1$, such as accompanied the ground state, have not yet appeared on the physical sheet. This and similar observations that may be made concerning Fig. 13 lead us to the following physical picture for high $\mathcal{B}$: for the $p$th band edge the state lying closest to the $p$th Landau level, a little below the band edge, will be $n=1, m=1-p$, the geometrically most confined state belonging to this level. It will have the exact symmetry $\lambda=i^{(1-p)}$. States with $1-p<m\leq 0$ and $n=p-|m|$, since they are larger in radial extent, will have $kw$ values lying above this state, perhaps on the second sheet. States with positive $m$ appropriate to this Landau level may also appear, to the extent that the $m\leq 0$ states have room to translate in any direction and not collide significantly with the walls of the junction. Their presence and proximity in $kw$ value permits the construction of Landau states translated from the center of the junction.

Comparing Figs. 7 and 13 (parabolically confined channels give similar patterns[12]) we see that each of the valleys and "extra plateaux" of Fig. 7 is associated with one of the poles of Fig. 13. Poles whose positions have small imaginary parts generate valleys that widen out into plateaux as the imaginary part becomes large at smaller $\mathcal{B}$. The poles which contribute significant structure to $\mathcal{R}$ appear to be those that occur at low $\mathcal{B}$ for a given band, at a $kw$ well distinct from the band edge. For higher bands, and for $kw$ well above the band edge, the relevant value of $p_i w$, proportional to the velocity of the particle along the channel, is large, and the sideways Lorentz force produces orbits obeying the "turn-right" rule. One does not expect large overlap between such scattering states (which tend to stay near the edge of the channel) and the kind of resonant states we have examined (which are symmetrically located about the center of the junction), except when the velocity is low, which occurs just above the band edge. This gives a physical explanation of one of the results of Fig. 13, which shows the states as being confined by the Landau levels and the band edges to a region of $kw$ that decreases as $\mathcal{B}\rightarrow\infty$. One thus expects in $\mathcal{R}$ a structure, which for high $\mathcal{B}$ is confined narrowly to the band edges, and may become self-canceling, as states with $\lambda$ values of both $i$ and $-i$ are concentrated in this range of $\mathcal{B}$.

### B. Tees and elbows

The scattering probabilities for the four-terminal junction of Fig. 1 as well as the tees ("T") and elbows ("L") of Fig. 4 made from it by removing some of the arms are recorded in Fig. 14 for the value $\mathcal{B}=6.0$ and a range of $kw$ covering the opening of four channels. We plot

$$S_R=\sum_{n'} S_{Rn'n},\quad S_L=\sum_{n'} S_{Ln'n},\quad F=\sum_{n'} F_{n'n},\quad R=\sum_{n'} R_{n'n},$$

with $n=1$, i.e., the incident wave is only in the lowest open channel.

Dominant features for most of the junctions are the cusp structures near the opening of new channels at $kw$ close to multiples of $\pi$ and resonances just below these thresholds. The variations near $kw=5.6$ and 9.2 for the full four-point junction, discussed earlier as a manifestation of resonant virtual levels with exact symmetries $\lambda=-i$ and $i$, respectively, are for the amputated junctions either shifted in $kw$ or are absent , a not unreasonable result of modifying the confining potential.

It is seen from Fig. 14(a) that for the full junction, the left-turn arm contributes $\lesssim 10\%$ to the overall process. It is therefore reasonable that for the tee junction [Fig. 14(d)], which lacks a left-turn arm, the remaining probabilities are very similar to those of the full junction. A similar interpretation applies to the tee junction [Fig. 14(c)], which has a left-turn arm but no right-turn arm, and for which, except at thresholds, there is only forward scattering. At the simple elbows [Figs. 14(e) and 14(f)], there is mainly left or right scattering until the second threshold at $kw\simeq 6.3$. Thereafter, they both cause significant reflection, with variations that are quite $kw$

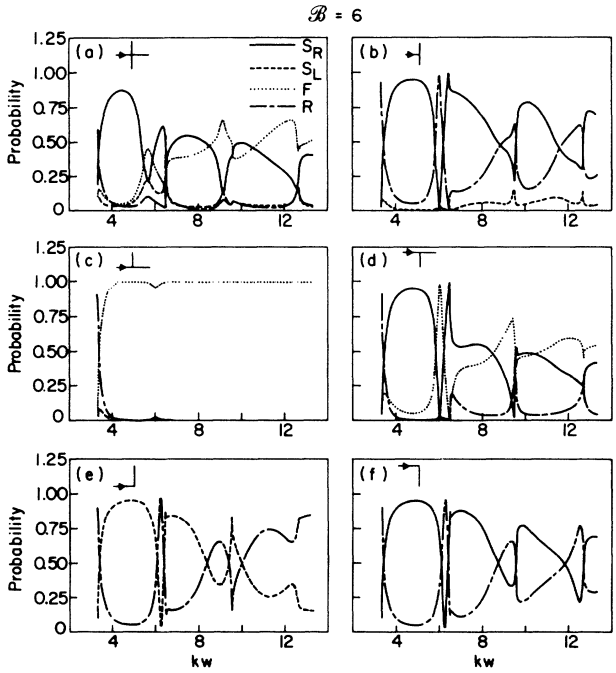


FIG. 14. Scattering probabilities as a function of $kw$, for $\mathcal{B}=6.0$, according to the convention $S_R$ (right scattering), solid line; $S_L$ (left), dashed; $F$ (forward), dotted; and $R$ (backward), chain dash; for (a) the four-terminal junction; (b)–(d), the tee ("T") junction with the three possibilities for incident waves; (e) and (f), the elbow ("L") with the two possibilities for incident waves. The line convention is the same throughout.

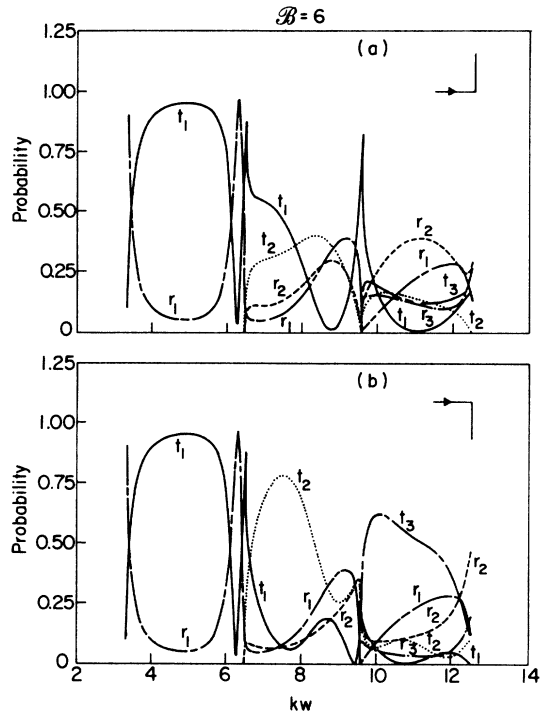


FIG. 15. Intermode scattering probabilities for the elbow ("L") junction as a function of $kw$ for $\mathcal{B}=6.0$, according to the convention that left or right scattering into mode $m$ is labeled $t_m$ (for transmission), and backward scattering is $r_m$ (for reflection); the incident beam has mode $m=1$. (a) Left-turn elbow; (b) right-turn elbow.

dependent. Up to the third threshold $kw \simeq 9.5$ the total scattering probabilities are remarkably similar for left and for right elbows; at larger $kw$ values they start to differ significantly. It is important to note this fact: inclusion of elbows or other abrupt changes in shape have nonignorable effects on the scattering probabilities of the circuit, and therefore on its resistive properties.

In anticipation of the possibility of more detailed experiments in the ballistic regime that permit the detection of individual mode occupation probabilities (as distinct from summing over all modes in obtaining the Hall resistance) we show in Fig. 15 the probabilities that a particle incident on either of these elbows in the mode $m=1$ scatters or reflects into other open modes. It is clear that in the region $6.3 \lesssim kw \lesssim 9.4$, where just two outgoing modes are open, the left and right elbows differ markedly in this intermode scattering, whereas the total scattering in that region, as seen in Figs. 14(e) and 14(f), is very similar for the two junctions. Although brevity does not allow further display, such results pertain to all of the junctions we shall discuss: intermode scattering reflects more sensitively than total scattering the characteristics of any of the configurations we examine.

### C. Six terminals and higher

Figure 16 gives some results for the six-terminal junction of Fig. 5(a), which might be said to be a closer approximation to actual Hall-effect circuits than the four-terminal junction customarily discussed. In our calculation the current flows between arms 1 and 6, with no current in arms 2–5. Figure 16 gives the transverse Hall resistance $R_{32}$ and the longitudinal resistance $R_{35}$. From

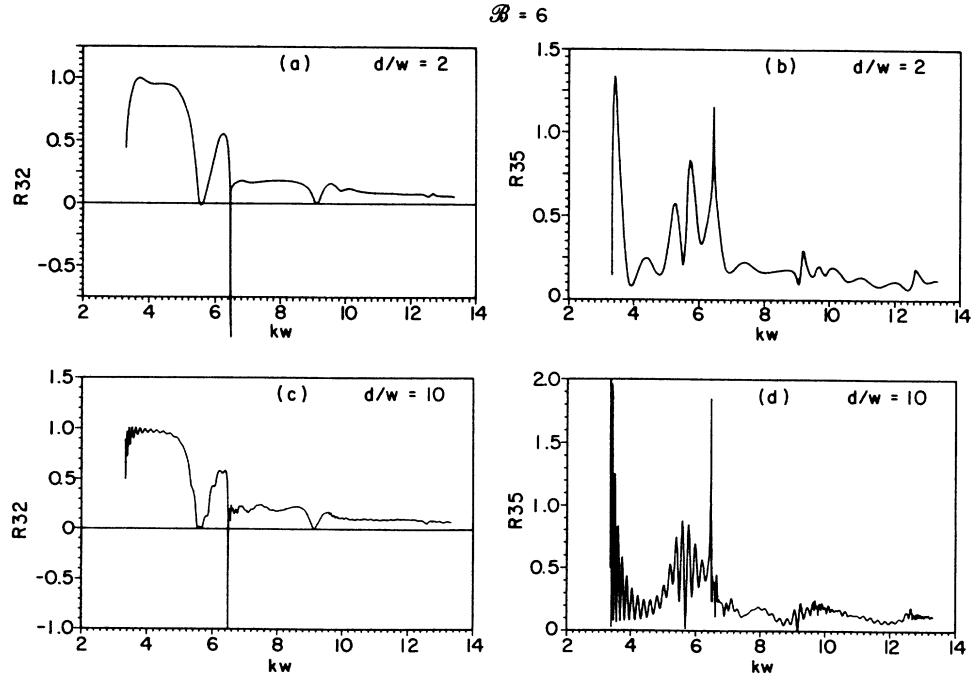


FIG. 16. Resistance for the six-terminal junction of Fig. 5(a) [with separation $d/w=2.0$, in (a) and (b) and $d/w=10.0$ in (c) and (d)] as a function of $kw$ for $\mathcal{B}=6.0$: (a) and (c) the Hall resistance $R_{23}$; (b) and (d) the longitudinal resistance $R_{35}$.

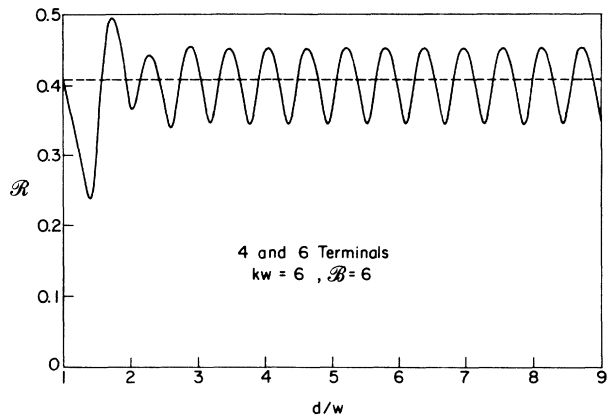


FIG. 17. The Hall resistance $R_{23}$ for the six-terminal junction (solid line) compared to its value for the four-terminal junction (dashed line) as a function of the separation $d/w$, for $kw=6.0$ and $\mathscr{B}=6.0$.

rotational invariance the two possible transverse Hall resistances $R_{32}$ and $R_{54}$ are equal. In Figs. 16(a) and 16(b) $d/w$, the distance between junctions divided by the width of the arms, is 2, and in Figs. 16(c) and 16(d) $d/w=10$. Comparing the Hall resistance graphs Figs. 16(a) and 16(c) with Fig. 9(a), the corresponding Hall resistance plot for the four-terminal junction, we see the appearance of oscillations. These are due to interference effects in the arm connecting the two junctions, and are clearly very dependent on the ratio $d/w$.

Figure 17 compares the Hall resistance for the four- and six-terminal junctions as a function of $d/w$ for values $kw=6$ and $\mathscr{B}=6$. At small values of $d/w$, evanescent modes can reach between the left and right junctions and influence the interference pattern. At larger $d/w$, only the one open mode contributes. In this region of $kw$ and $\mathscr{B}$ one presumably wishes to explore the four-terminal behavior and its dependence on the adjacent threshold and the Landau level. Yet depending on the precise value of the separation $d/w$, the Hall resistance fluctuates markedly about the "theoretical" four-terminal value. It is true that so far as actual measurements are concerned, irregularities in the character of the potential and in the geometry may prevent one from knowing the effective value of $d/w$ being used. Such uncertainty does not mean that there are not interference effects of the magnitude that we show, but that their precise phase (location on the wiggle) is unknown. It is important to be aware of this ambiguity, although we do not as yet know how to remedy it. If the spacing $d$ is longer than the impurity-scattering mean free path, of course, the phase coherence that causes the oscillations may cancel, so that what is measured will more resemble the average value of the ballistic calculation.

Table III lists the Hall resistances $R_{32}, R_{54}, R_{76}, \ldots,$ for $n$-terminal linear arrays as in Fig. 6(a) with various numbers of terminals at $\mathscr{B}=6.0$, $d/w=2.0$, and two values of $kw$. The current flows from arm 1 to arm $n$ with no current in the transverse arms. These results were calculated with the iterative scheme of Sec. III C. We note that for more than six terminals rotational invariance does not imply equality for all the Hall resistances, and they are in fact not all equal. The measured Hall resistance depends on which arms are used.

### D. Loop circuit

The square loop circuit, with wires a distance $d$ apart measured from the centers, is shown again in the inset to Fig. 18(a) to define the terminal locations. In the particular, rather symmetrical case we consider, unit current

TABLE III. Hall resistances for the $n$-terminal arrays of Fig. 6(a). $\mathscr{B}=6.0, d/w=2.0$. The numerical accuracy of the calculation is one part in the last digit shown. Rotational invariance says each horizontal line of the table should be symmetric about its center.

| $kw$ | $n$ | $R_{32}$ | $R_{54}$ | $R_{76}$ | $R_{98}$ | $R_{11,10}$ | $R_{13,12}$ | $R_{15,14}$ | $R_{17,16}$ | $R_{19,18}$ |
|---|---|---|---|---|---|---|---|---|---|---|
| 10.0 | 4 | 0.1198 | | | | | | | | |
| | 6 | 0.1210 | 0.1210 | | | | | | | |
| | 8 | 0.1203 | 0.1208 | 0.1203 | | | | | | |
| | 10 | 0.1203 | 0.1216 | 0.1215 | 0.1203 | | | | | |
| | 12 | 0.1208 | 0.1222 | 0.1232 | 0.1222 | 0.1208 | | | | |
| | 14 | 0.1210 | 0.1225 | 0.1233 | 0.1233 | 0.1225 | 0.1209 | | | |
| | 16 | 0.1209 | 0.1227 | 0.1234 | 0.1231 | 0.1234 | 0.1226 | 0.1209 | | |
| | 18 | 0.1210 | 0.1227 | 0.1237 | 0.1233 | 0.1233 | 0.1237 | 0.1226 | 0.1209 | |
| | 20 | 0.1210 | 0.1227 | 0.1237 | 0.1236 | 0.1236 | 0.1236 | 0.1237 | 0.1226 | 0.1209 |
| 14.0 | 4 | 0.0575 | | | | | | | | |
| | 6 | 0.0697 | 0.0697 | | | | | | | |
| | 8 | 0.0775 | 0.0809 | 0.0775 | | | | | | |
| | 10 | 0.0751 | 0.0888 | 0.0888 | 0.0750 | | | | | |
| | 12 | 0.0756 | 0.0865 | 0.0967 | 0.0864 | 0.0756 | | | | |
| | 14 | 0.0762 | 0.0869 | 0.0944 | 0.0944 | 0.0869 | 0.0761 | | | |
| | 16 | 0.0759 | 0.0875 | 0.0948 | 0.0920 | 0.0948 | 0.0874 | 0.0758 | | |
| | 18 | 0.0760 | 0.0872 | 0.0953 | 0.0925 | 0.0925 | 0.0953 | 0.0872 | 0.0759 | |
| | 20 | 0.0760 | 0.0873 | 0.0951 | 0.0930 | 0.0929 | 0.0930 | 0.0951 | 0.0872 | 0.0759 |

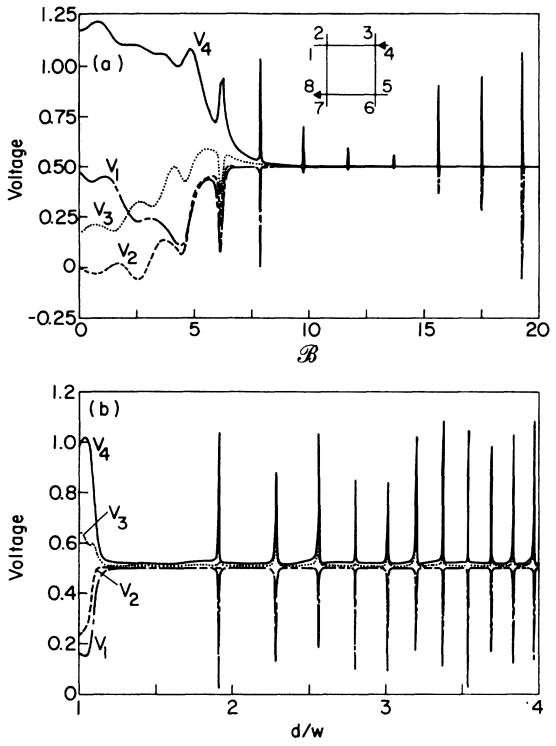


FIG. 18. Voltages of various leads of the square loop circuit for $kw=5.0$. The current flow and the numbering of the leads are shown in the inset. The curve conventions are: $v1$, long-dash short-dash curve; $v2$, dashed; $v3$, dotted; $v4$, solid. The average of the lead voltages is defined to be zero, so that by rotational symmetry $v8=-v4$, $v7=-v5$, etc. (a) Voltage as a function of $\mathcal{B}$ for $d/w=1.95$; (b) voltage as a function of $d/w$ for $\mathcal{B}=8.0$.

enters in arm 4 and leaves from arm 8, and there is zero current in the other external arms. The voltages for a square loop, $d/w=1.95$, for $kw=5.0$, are shown as a function of $\mathcal{B}$ in Fig. 18(a). At low $\mathcal{B}$ the Aharonov-Bohm oscillations are seen as sinusoidal changes superimposed on slower fluctuations similar to those of the four-terminal junction as in Fig. 8. As the Hall plateau ($V=0.5$ corresponds to $\mathcal{R}=1.0$) is approached these sinusoidal oscillations become much sharper, more resonance like in shape and, at large $\mathcal{B}$, are extremely narrow. Finite-temperature averaging is likely to make these resonances difficult to observe experimentally. Thus the Aharonov-Bohm oscillations observable at low $\mathcal{B}$ are likely to be washed out at high $\mathcal{B}$. Experiments on circular loops[18,19] show effects similar to these.

The analytic treatment of the loop problem in Sec. III E helps to understand the periodicity of these resonances. We note, referring to Fig. 2, that there is only one open channel, and from Fig. 7 that the characteristics of the four-terminal junctions forming the corners of the square are free of rapid fluctuations in this region. We recall that our analytic treatment in Sec. III E encompasses the possibility of resonant behavior. Following the arguments given there, we expect that an internal wave of large amplitude circulating around the square would suffer a phase shift $\delta_R$ on turning right at a corner, the phase acquired along each arm would be $p_1 d$ (since only mode 1 has a traveling wave), so that together with the Aharonov-Bohm phase $-\mathcal{B}(d/w)^2$ the total phase accumulation around the square is $4(\delta_R+p_1 d)-\mathcal{B}(d/w)^2$. The condition for large internal waves is that this phase is a multiple of $2\pi$. For fixed $k$ and $\mathcal{B}$, the phase $\delta_R$ and the longitudinal momentum $p_1$ are fixed, so that the total phase is quadratic in $d/w$. To verify this hypothesis we show in Fig. 18(b) the voltages of the same square, and again $kw=5$, but for fixed $\mathcal{B}=8$ as a function of $d/w$. The resonant positions show this quadratic dependence on $d/w$, for fixed $\mathcal{B}$.

Similarly, by making $d/w$ larger the $\mathcal{B}$ dependence of this total phase accumulation becomes dominated by the $-\mathcal{B}(d/w)^2$ term, i.e., $\delta_R$ and $p_1$ can be considered slowly varying functions of $\mathcal{B}$. In such a case the oscillation spacing is approximately $\Delta\mathcal{B}\cong 2\pi(w/d)^2$. In Fig. 19(a) we show the same voltages as in Fig. 18(a) but for $d/w=6.0$ instead of 1.95. The oscillation frequency is much higher and again the resonances become very narrow in the region of the plateau.

Aharonov-Bohm oscillations are often described in terms of the amount of flux enclosed by the closed orbit of the electron $\phi=\mathcal{B}$ (area/$w^2$). Since the channel width is finite the area enclosed by the square loop is ambiguous, lying between $(d-w)^2$ and $(d+w)^2$. One might expect this spread in areas to show up as a spread in the oscillation frequencies[20] of the Aharonov-Bohm oscillations in Figs. 18(a) and 19(a). We show in Figs. 19(c) and 19(d) the Fourier decomposition of $V_2(\mathcal{B})$ and $V_4(\mathcal{B})$. The frequency (area) is very well defined at $(5.86\pm0.05w)^2$ indicating that the electron orbit is effectively very close to the center of the channels [at the center the area $=d^2=(6w)^2$]. The case shown has $kw=5.0$ so that only one propagating mode is present. At higher $kw$, where more modes propagate, one might expect more spread in effective area corresponding to the spread in the effective areas of the differing modes, but it will probably not show the full width of the channel. In Fig. 19(b) are shown the voltages for $d/w=6.0$ but with $kw$ raised to 11.0, where three modes propagate. The corresponding Fourier decompositions of $V_2(\mathcal{B})$ and $V_4(\mathcal{B})$ are shown in Figs. 19(e) and 19(f). Arrows indicate the frequencies expected when the effective area corresponds to the inside $(5w)^2$, centerline $(6w)^2$, and outside $(7w)^2$ of the square loop. The spectrum is wider than at $kw=5.0$ [Fig. 19(c)] but by no means does it cover the full width of the channel. Attempts at determining the channel width for real devices by measuring the spread in Aharonov-Bohm oscillation frequencies for circular loops yield smaller widths than other methods.[18-20] Our results demonstrate that such a method does not determine well the physical width of the channels.

Looking at the voltage curves of Figs. 18(a), 19(a), and 19(b) we note that peaks (or valleys, depending on the two arms chosen to measure the voltage) of varying sharpness can be obtained, according to whether $\mathcal{B}$ is such that the basic four-terminal junction is operating on the Hall plateau or in the foothills. Additionally, one might expect, by operating at higher $kw$ values, to exploit

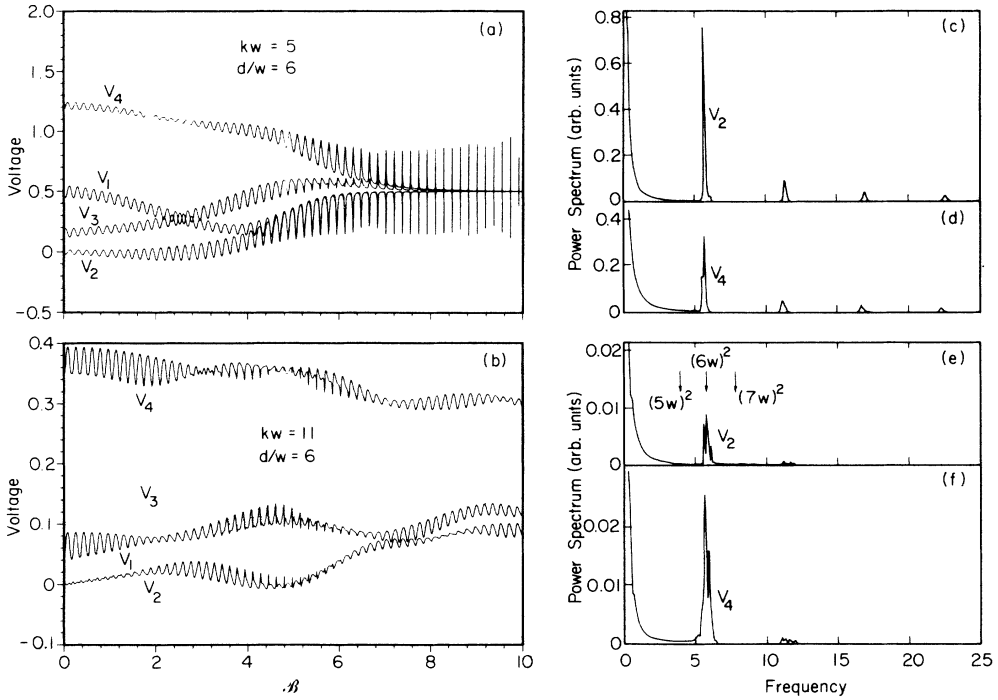


FIG. 19. Voltages for unit current through a square loop as in Fig. 18 but for $d/w=6.0$. On the left are shown the voltages as a function of $\mathcal{B}$ for (a) $kw=5.0$, where only one submode is open and (b) $kw=11.0$, where three submodes are open. On the right the fourier power spectra of some of the curves on the left are shown: (c) and (d) are for curves $V_2$ and $V_4$ of the $kw=5$ case, while (e) and (f) are the same curves for $kw=11$. The arrows in (e) show the frequency expected for Aharonov-Bohm oscillations when the effective area corresponds to the inside $(5w)^2$, center line $(6w)^2$, and outside $(7w)^2$ of the loop. Frequency is given in oscillations per unit change of $\mathcal{B}$.

a combination of the resonances of the basic four-terminal junction with these resonances of the loop. There are many possibilities which could be experimentally and theoretically investigated.

## V. CONCLUSION

We have presented extensive calculations in the ballistic approximation, i.e., noninteracting electrons, for the scattering probabilities and from these the Hall resistance, in two-dimensional circuits of rectangular segments that form junctions connected by narrow channels with infinite walls, in a magnetic field perpendicular to the plane of the circuit. The calculations proceed in two stages. First, we calculate the detailed amplitudes of the four-terminal junction with one intersection. These amplitudes are then combined in the appropriate way to find the scattering amplitudes and probabilities for multiterminal junctions with several intersections. These calculations depend on the two dimensionless parameters $kw=(2m^*Ew^2/\hbar^2)^{1/2}$ and $w/l=(qB/\hbar c\times w^2)^{1/2}$, so that for narrow wires quantum effects become important.

With noninteracting electrons many aspects of the Hall effect, e.g., the fractional Hall effect, are of course absent. Nonetheless, we find a rich structure that results from the elementary physics of wave interference as contained in the Schrödinger wave equation and infinite wall boundary conditions describing the system. We have succeeded in understanding much of the complex structure present in the results as due to the influence of particular quantum states, which we can identify in the large-$B$ limit with Landau levels pinned at the intersections. Other effects are due to interference in the arms connecting intersections.

The results presented here have been obtained with an idealized shape for the confining potential, namely an infinite square well with 90° corners between the arms. Some of the details of the resistance curves will depend on the specific shape. On the other hand, we believe the existence of resonances associated with pinned Landau levels is likely to be independent of the details of the geometry, as are the oscillations and narrow resonances associated with propagation around closed loops and the influence of reflections from nearby arms and elbows. Some results with a parabolic confining potential have been reported by Kirczenow.[12] The influence of tapered arms has been discussed by Baranger and Stone,[13] particularly in the context of quenching of the Hall resistance. Rounding of the 90° corners has been investigated experimentally by Ford *et al.*[6] and by Chang *et al.*[7] (Except for the work of Baranger and Stone, very little theoretical attention has as yet been given to the corners.) Together these show that the geometry does influence the details, but that common features are present.

We have two points of interest: (1) Although other

conductance mechanisms could be important for a complete understanding of real experimental data, much of the complex structure of the data can be accounted for by quantum interference effects of the sort we have calculated and these interference effects should be included in any analysis of experimental data. (2) Since interference effects in the arms significantly change our results, the external leads in real experimental equipment are not passive objects. Their influence, which depends sensitively on the geometry, must be calculated as we have done here.

## ACKNOWLEDGMENTS

We are indebted for suggestions and encouragement to several people: M. Büttiker, S.-J. Chang, R. Landauer, J.-P. Leburton, M. L. Roukes, and M. Stone. The computations presented were made in part on the Cray Research, Inc. X-MP/48 computer at the National Center for Supercomputing Applications, Urbana, Illinois. The research was supported in part by National Science Foundation (NSF) grants No. PHY-84-15064 and No. PHY-87-01775.

[1]M. L. Roukes, A. Scherer, S. J. Allen, Jr., H. G. Craighead, R. M. Ruthen, E. D. Beebe, and J. P. Harbison, Phys. Rev. Lett. **59**, 3011 (1987).

[2]J. A. Simmons, D. C. Tsui, and G. Wiemann, Surf. Sci. **196**, 81 (1988).

[3]G. Timp, A. M. Chang, P. Mankiewich, R. Behringer, J. E. Cunningham, T. Y. Chang, and R. E. Howard, Phys. Rev. Lett. **59**, 732 (1987); A. M. Chang, G. Timp, T. Y. Chang, J. E. Cunningham, P. M. Mankiewich, R. E. Behringer, and R. E. Howard, Solid State Commun. **67**, 769 (1988); G. Timp, H. U. Baranger, P. deVegvar, J. E. Cunningham, R. E. Howard, R. Behringer, and P. M. Mankiewich, Phys. Rev. Lett. **60**, 2081 (1988).

[4]C. J. B. Ford, T. J. Thornton, R. Newburg, H. Ahmed, D. C. Peacock, D. A. Ritchie, J. E. F. Frost, and G. A. C. Jones, Phys. Rev. B **38**, 9375 (1988); C. J. B. Ford, T. J. Thornton, R. Newburg, M. Pepper, H. Ahmed, D. C. Peacock, D. A. Ritchie, J. E. F. Frost, and G. A. C. Jones, *ibid.* **38**, 8518 (1988).

[5]Y. Takagaki, K. Gamo, S. Namba, S. Takaoka, K. Murase, S. Ishida, K. Ishibashi, and Y. Aoyagi, Solid State Commun. **69**, 811 (1989); Y. Takagaki, K. Gamo, S. Namba, S. Ishida, S. Takaoka, K. Murase, K. Ishibashi, and Y. Aoyagi, *ibid.* **68**, 1051 (1988).

[6]C. J. B. Ford, S. Washburn, M. Büttiker, C. M. Knoedler, and J. M. Hong, Phys. Rev. Lett. **62**, 2724 (1989); C. J. B. Ford, S. Washburn, M. Büttiker, C. M. Knoedler, and J. M. Hong, Surf. Sci. (to be published).

[7]A. M. Chang, T. Y. Chang, and H. U. Baranger, Phys. Rev. Lett. **63**, 996 (1989).

[8]M. Büttiker, Phys. Rev. Lett. **57**, 1761 (1986); M. Büttiker, IBM J. Res. Dev. **32**, 317 (1988).

[9]F. M. Peeters, Phys. Rev. Lett. **61**, 589 (1988).

[10]D. G. Ravenhall, H. W. Wyld, and R. L. Schult, Phys. Rev. Lett. **62**, 1780 (1989).

[11]Y. Avishai and Y. B. Band, Phys. Rev. Lett. **62**, 2527 (1989).

[12]G. Kirczenow, Phys. Rev. Lett. **62**, 2993 (1989).

[13]H. U. Baranger and A. D. Stone, Phys. Rev. Lett. **63**, 414 (1989).

[14]*The Quantum Hall Effect,* edited by R. R. Prange and S. M. Girvin (Springer-Verlag, New York, 1987).

[15]M. Büttiker, Phys. Rev. B **38**, 12724 (1988).

[16]R. L. Schult, D. G. Ravenhall, and H. W. Wyld, Phys. Rev. B **39**, 5476 (1989).

[17]L. D. Landau and E. M. Lifshitz, *Quantum Mechanics,* Vol. 3 of Course in Theoretical Physics, 3rd ed. (Pergamon, New York, 1977), pp. 456–459.

[18]G. Timp, A. M. Chang, J. E. Cunningham, T. Y. Chang, P. Mankiewich, R. Behringer, and R. E. Howard, Phys. Rev. Lett. **58**, 2814 (1987).

[19]C. J. B. Ford, T. J. Thornton, R. Newbury, M. Pepper, H. Ahmed, C. T. Foxon, J. J. Harris, and C. Roberts, J. Phys. C **21**, L325 (1988).

[20]R. A. Webb, S. Washburn, C. P. Umbach, and R. B. Laibowitz, Phys. Rev. Lett. **54**, 2696 (1985).